IL6 and CCL18 Mediate Cross-talk between *VHL*-Deficient Kidney Cells and Macrophages during Development of Renal Cell Carcinoma

Thi-Ngoc Nguyen[1,2], Hieu-Huy Nguyen-Tran[1,2], Chen-Yun Chen[1], and Tien Hsu[1,2]

ABSTRACT

Loss of the *von Hippel–Lindau* (*VHL*) tumor suppressor gene function accounts for 70% to 80% of all clear-cell renal cell carcinoma (ccRCC) cases, the most prevalent form of RCC. Accumulating evidence has indicated that ccRCC arises from sites of chronic inflammation, yet how ccRCC tumor cells interact with immune components of the microenvironment has not been fully elucidated. In this study, we used unbiased proteomic and genomic analyses on components of the tumor microenvironment under different conditions, identifying the molecular and cellular mechanisms that underlie the cross-talk between *VHL*-deficient kidney tubule cells and macrophages. *In vitro* and in a *Vhlh* conditional knockout mouse model, *VHL*-deficient noncancerous kidney epithelial cells, representing the early stage of ccRCC initiation, secreted IL6 that induced macrophage infiltration and polarization toward the protumorigenic M2 phenotype. Activated human macrophages secreted CCL18 and TGFβ1 to stimulate epithelial-to-mesenchymal transition (EMT) of the kidney tubule cells. Treatment with IL6-neutralizing antibody rescued inflammatory, proliferative, and EMT phenotypes of kidney epithelial cells in *Vhlh* conditional knockout mice. Furthermore, in a human ccRCC xenograft model, exogenous human primary or cultured macrophages significantly promoted primary tumor growth and metastasis in a CCL18-dependent manner. These findings identify specific factors involved in reciprocal cross-talk between tumor cells and immune components in the microenvironment, thus providing an avenue for early intervention in ccRCC.

Significance: The identification of *VHL*-deficient kidney tubule cell cross-talk with macrophages regulated by IL6 and CCL18 reveals potential targets for the prevention and treatment of ccRCC.

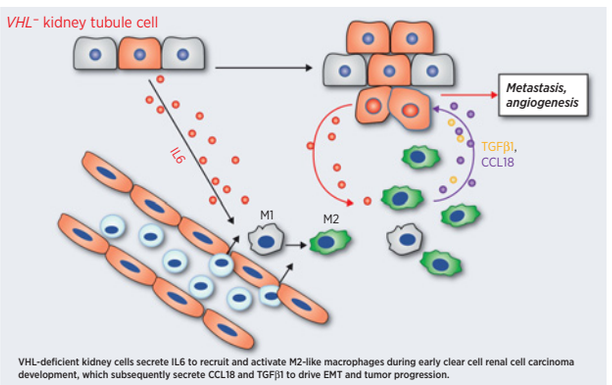

VHL-deficient kidney cells secrete IL6 to recruit and activate M2-like macrophages during early clear cell renal cell carcinoma development, which subsequently secrete CCL18 and TGFβ1 to drive EMT and tumor progression.

Introduction

Kidney cancer is a worldwide health concern. According to the World Health Organization, there were 403,262 new cases diagnosed in 2018 (up from 337,860 in 2012; a 19% increase), and 175,098 deaths (up from 143,406 in 2012; a 22% increase). About 90% of all kidney cancers are renal cell carcinoma (RCC; refs. 1, 2), among which clear-cell RCC (ccRCC) is the most common histologic subtype and accounts for the most kidney cancer-related deaths (2). ccRCC is resistant to radiation and chemotherapy and shows a high rate of recurrence after targeted tyrosine kinase inhibitor therapy (3). Unlike other more prevalent cancers such as those of prostate and breast, ccRCC incidences and deaths continue to rise for uncertain reasons. Therefore, additional therapeutic and diagnostic approaches are needed.

Genetic and epigenetic defects in the *VHL* tumor suppressor gene are associated with up to 80% of all ccRCC cases (4) and are considered the driver of a majority of ccRCC (5–7). The VHL protein is the substrate recognition component of the E3 ubiquitin ligase complex that mediates the ubiquitination and degradation of hypoxia-inducible factor-α (HIFα; ref. 8). However, because unlike other tumor suppressors such as *TP53* and *Rb*, *VHL* is not directly involved in apoptosis or cell-cycle regulation, the pathologic process by which a *VHL*-deficient kidney epithelial cell initiates tumor formation is still not entirely clear.

Accumulating evidence has linked tissue inflammation with the development of many forms of cancer, including ccRCC (9–12). Also, recent advances in the understanding of the tumor microenvironment suggest that the interaction between tumor cells and infiltrating immune cells plays a dynamic role in tumorigenesis. Relevant to these concepts, previously, our laboratory has demonstrated that *VHL*-deficient epithelial cells exhibit unfolded protein response and endoplasmic reticulum (ER) stress that in turn induce inflammatory

[1]Department of Biomedical Sciences and Engineering, National Central University, Taoyuan City, Taiwan, Republic of China. [2]Graduate Institute of Biomedical Sciences, China Medical University-Taiwan, Taichung, Taiwan, Republic of China.

Corresponding Author: Tien Hsu, Graduate Institute of Biomedical Sciences, China Medical University-Taiwan, No. 91, Hsueh-Shih Rd., Taichung, Taiwan 40402, Republic of China. Phone: 220-53366-8210; E-mail: tienhsu@mail.cmu.edu.tw

Cancer Res 2022;82:2716–33

doi: 10.1158/0008-5472.CAN-21-3749

responses in the stroma and hyperplasia in the tubule cells (13). However, the exact molecular and cellular mechanisms underlying the cross-talk between *VHL*-deficient cells and the microenvironment have remained unresolved. It is also unclear whether *VHL*-deficient cells are simply a target for the infiltrating immune cells or are an active player that initiates the reconstitution of inflammatory and tumorigenic microenvironment. This is an important question, because if the latter is true, it may be possible to break the signaling events and prevent tumor growth at the earliest stage of tumorigenesis.

Among the cellular components in the tumor microenvironment, macrophages are a key player in modulating the immune responses linking inflammation and cancer formation (14–16). Macrophages display a plasticity that can adopt different functionalities constituting a contiguous spectrum, which is traditionally characterized by classically activated M1 and alternatively activated M2 subtypes at the two ends of the spectrum (17). As the tumor progresses, the tumor-associated macrophages (TAM) are enriched in populations exhibiting a protumor function associated with the M2 phenotype (18, 19). Consistent with these findings, M2-type TAM infiltration is often associated with poor prognosis (15).

Previously, our laboratory generated a mouse model of conditional knockout (KO) of *Vhlh* (mouse genomic locus of the *VHL* gene) in subpopulations of the kidney tubules using the *Hoxb7-Cre-GFP* driver. The conditional KO results in tissue inflammation, fibrosis, cyst formation, appearance of abnormal clear cells, and hyperplasia, without the formation of malignant tumor (13, 20). Importantly, the *Vhlh* KO phenotypes, including hyperplasia, can be alleviated by the treatment with the cytokine signaling inhibitors ruxolitinib and tofacitinib (20, 21). As such, this model represents an early-stage development of ccRCC and suggests that the inflammatory microenvironment may play an important role in ccRCC formation.

Macrophage infiltration in the inflammatory microenvironment has been observed in previous studies of ccRCC models containing *VHL* mutations (15, 20, 22, 23). It is, therefore, reasonable to posit that *VHL*-deficient epithelial cells can induce infiltration and activation of macrophages, and these activated macrophages may play an important role in stimulating the progression of the tumor.

In this study, we aim to understand the interactive mechanism that underlies the cross-talk between the *VHL*-deficient kidney tubule cells and the macrophages with relevance to ccRCC formation. The results show that *VHL/Vhlh*-deficient kidney tubule cells secret IL6 that induces infiltration of macrophages and promotes their polarization toward the traditionally defined M2 phenotype. In the reciprocal action, the activated macrophages expedite tumor progression by secreting at least CCL18 and TGFβ1 to induce growth and mesenchymal transition of the kidney tubule cells. Furthermore, macrophages expressing CCL18 are critical in promoting ccRCC growth and metastasis in a xenograft model. These results thus suggest an avenue for early detection and treatment of ccRCC.

Materials and Methods

A detailed description of cellular and biochemical experiments is described in Supplementary Materials and Methods. Antibodies used in flow cytometry, immunohistochemistry (IHC), Western blotting, and neutralization are listed in Supplementary Table S1 with experimental conditions. The culture media and reagents are listed in Supplementary Table S2. The primers for quantitative RT-PCR are listed in Supplementary Table S3.

Cell culture

All cell lines used were purchased from cell line repositories (ATCC or Bioresource Collection and Research Center) that provide authentication. Upon receiving the samples from the suppliers, the cells were grown to ∼70% to 80% confluency, expanded, examined for the presence of contaminating *Mycoplasma* using EZ-PCR Mycoplasma Detection Kit (from Biological Industries, SKU: 20-700-20), and stored in liquid nitrogen according to standard protocols. Depending on the proliferative characteristics of the cell lines, the expanded cells were rinsed and divided into 15–30 one-mL aliquots, each containing the number of cells equivalent to ∼25% to 40% confluency in a 100-mm dish. Each frozen aliquot was used and propagated for no more than 10 passages. A portion of the regrown cells was stained with DAPI to ensure the lack of *Mycoplasma* contamination. Other experimental details are described in Supplementary Materials and Methods.

Animal models and human kidney samples

The conditional KO of *Vhlh* (with exon 1 deleted) has been described previously (13, 20, 24). Briefly, the KO mouse strain *Hoxb7-Cre-GFP/+*; $Vhlh^{loxP/loxP}$ of the C57BL/6 background was generated by intercross of *Hoxb7-Cre-GFP/+*; $Vhlh^{loxP/+}$. Littermates with the genotype *Hoxb7-Cre-GFP/+* or $Vhlh^{loxP/loxP}$ served as wild-type controls. *Hoxb7-Cre-GFP* is a *Hoxb7* promoter-driven Cre line with a GFP reporter. Phenotypic analyses were performed on 3-month-old mice. For the phenotypic rescue experiment, 2-month-old mice were injected intravenously (i.v.) with an αIL6-neutralizing antibody (100 μg/mouse) every week for 4 weeks. The dosage used was based on the published protocol (25).

The immune-deficient NOD/SCID mouse strain was purchased from BioLASCO Taiwan. Two-month old animals were used for xenograft experiments.

Human paraffin-embedded tissue array was purchased from Biomax (KD241) and archived human ccRCC (containing *VHL* loss of heterozygosity) samples were collected from patients at Tri-Service General Hospital, Taiwan, with IRB approval (no. 2-106-05-079), which are *VHL* mutant. Other mutations are not known, but we have not observed significant variations in the phenotypes we examined.

ccRCC xenograft

The protocol for 786-O cell implantation was adapted from Nguyen-Tran and colleagues (21) with modifications. Prior to implantation, NOD/SCID mice were treated with 1 mg (in 200 μL) clodronate-containing liposomes (Liposoma BV, SKU: C-010) every 2 days for 6 days (three times) by i.v. injection. 5×10^5 786-O cells expressing luciferase (786-O^{Luc}; 786-O only group) or a mixture of 4.5×10^5 786-O^{Luc} cells and 0.5×10^5 human peripheral blood-derived $CD14^+$ monocytes (PBMCs) or THP-1 cells (with or without *CCL18* KD) were prepared in a 10-μL solution of cold serum-free RPMI medium and growth-factor-reduced Matrigel (Corning 356231) at a 1:1 ratio.

Two days after the clodronate treatment, mice were anesthetized, placed right lateral recumbency, and hair shaved from fore- to hind limbs. An ∼1-cm incision was cut in a longitudinal direction between the last rib and the hip joint to exteriorize the left kidney, followed by injection with 10 μL of cell suspension under the renal capsule membrane using the Hamilton syringe. The kidney was then returned to the body. The skin layer was pulled together and closed with 2–3 wound clips (UNIK-Braided Silk, SC126).

In the 786-O+PBMC or 786-O+THP-1 (with or without *CCL18* KD) group, 1×10^6 monocytes in 100 μL PBS were i.v. injected into

mice once per week for 4 weeks. In the 786-O alone group, 100 μL PBS was injected similarly as control. Tumor growth and metastasis were monitored every week for 4 weeks after implantation by bioluminescence using an XENOGEN IVIS 200 after intraperitoneal injection of luciferin (150 mg/kg, Biosynth). The mice were sacrificed at 4 weeks after tumor implantation. The metastatic 786-O^{LUC} cells to the lung were examined by staining with antihuman mitochondria antibody, and the metastatic foci (defined as cell clusters ≥20 μm, or equivalent to ∼≥10 cells) were counted.

Statistical analysis

The values are presented as means ± SEM. The statistical analysis was performed using unpaired two-tailed Student *t* test (two-group comparison) or one-way ANOVA with Tukey post hoc test (multiple-group comparison). The difference between groups was considered statistically significant when P value is < 0.05.

Data availability

The RNA-seq data have been deposited in the Gene Expression Omnibus (Accession # GSE183976). All other data and reagents generated in this study are available from the corresponding author upon request.

Results

Macrophages are abundant in human ccRCC samples and in the mouse kidney containing *Vhlh*-mutant tubule cells

Previously, we showed that the *Hoxb7-Cre-GFP*--driven *Vhlh* conditional KO mice exhibited a hyperplastic clear-cell phenotype accompanied by severe tissue inflammation and fibrosis in the kidney (13, 20). As the *Hoxb7-Cre* driver is marked with the GFP reporter, it is possible to examine more specifically the *Vhlh*-inactivated cells. Although *Hoxb7* has been described as a collecting duct-specific gene (26), the GFP-positive cells in *Hoxb7-Cre-GFP* transgenic line can be detected in the cortical region consisting of proximal and distal tubules (**Fig. 1A**). In the *Vhlh* KO animal, the GFP^+ tubule cells exhibit abnormal cell shape and epithelial piling-up (adenoma), and some begin to show clear-cell phenotype (**Fig. 1B**). In addition, an increased number of $CD45^+$ immune cells can be observed around the tubules containing *Vhlh* KO cells (**Fig. 1B** and **C**), compared with the wild-type (either $Vhlh^{loxP/loxP}$ without *Hoxb7-Cre-GFP* or *Hoxb7-Cre-GFP* without the $Vhlh^{loxP/loxP}$ allele). It has been shown that *VHL/Vhlh*-deficient cells require additional genomic changes for development into full-blown ccRCC (27, 28). As our KO mouse strain shows adenoma-like clear-cell lesions, but no malignant ccRCC, it represents a good model for specifically studying the early tumorigenic event. For brevity, in this report, we designate $Vhlh^{loxP/loxP}$ or *Hoxb7-Cre-GFP* as WT, and *Hoxb7-Cre-GFP;* $Vhlh^{loxP/loxP}$ as $Vhlh^{KO}$.

The extent of macrophage infiltration in human ccRCC clinical samples is analyzed with the macrophage marker CD68 (**Fig. 1D**). The result shows that there are very few macrophages in the normal adjacent tissue (NAT), but a dramatic increase of interstitial macrophages can be detected in the ccRCC proper. In the mouse $Vhlh^{KO}$ model, there are prominent inflammatory foci (dense clustering of immune cells; **Fig. 1E**). Most of these interstitial cells are macrophages as shown by IHC for the mouse pan-macrophage marker F4/80 (**Fig. 1F**). Overall, macrophages are enriched in the $Vhlh^{KO}$ kidney by ∼2.5-fold compared with WT (**Fig. 1G**).

Our ccRCC samples comprise ∼70% male, reflecting the known male prevalence of the disease (29). In our premalignant mouse model, there is no difference between male and female animals in the inflammatory phenotypes and extent of macrophage infiltration (Supplementary Fig. S1).

VHL-deficient kidney tubule cells induce macrophage extravasation and polarization toward the M2 phenotype

To test whether *VHL*-deficient kidney tubule cells can directly induce infiltration of macrophages, we used an *in vitro* extravasation assay. In this assay using the transwell chamber (with 8-μm pores in the polycarbonate membrane; **Fig. 2A**), the noncancerous human kidney tubule cell line HK-2, with or without *VHL* knockdown (KD), was plated in the lower chamber. The *VHL* KD efficiency of the shRNA constructs was monitored by protein blots (Supplementary Fig. S2A and S2B). Note that in these cellular assays we were interested in the inflammatory response at the early stage of ccRCC formation; therefore, the commonly used malignant ccRCC cell lines such as 786-O or A498, which have accumulated many additional genomic and epigenetic alterations, were not suitable for this purpose. In the upper chamber, human microvascular endothelial cells (HMEC) were labeled with live dye and plated first over the 0.1% gelatin-coated porous membrane, and allowed to grow to confluency mimicking the blood vessel wall (**Fig. 2B**). The partially differentiated macrophages derived from human monocyte precursor THP-1 cells [with 50 ng/mL phorbol 12-myristate-13-acetate (PMA)] were live-labeled and then added over the endothelial monolayer. These three cell types were cocultured for 48 hours before macrophage extravasation was assessed. As shown in **Fig. 2C** and **D**, a large number of transmigrated macrophages, but not endothelial cells, are detected in the presence of *VHL*-KD HK-2 cells (expressing *VHL*-specific shRNA: shVHL61 or shVHL3) compared with control (expressing shRNA of scrambled sequence, or shScr).

The traditional classification of M1 and M2 macrophages is overly simplified but still serves as a convenient criterion for broadly differentiating functionality. To understand the impact of *VHL*-deficient cells on differential activation of macrophages, we analyzed the macrophage phenotypes by flow cytometry after coculturing with HK-2 cells. In this assay (**Fig. 2E**), partially differentiated THP-1 cells were plated in the bottom well and cocultured with HK-2 cells (with or without *VHL* KD) in the upper well with a pore size of 0.4 μm (i.e., not passable by the HK-2 cells). After 48 hours, the macrophages were collected, and gated first for the $CD68^+$ population, followed by quantifying traditionally defined M1 (CD86) or M2 (CD163 or CD206) markers (**Fig. 2F**). In the presence of HK-2 control cells (expressing shRNA specific for *Luciferase*, shLuc), few $CD68^+$ macrophages differentiate into either M1 (∼1%–3% positive for CD86) or M2 (∼0.3% positive for CD206 or ∼2% positive for CD163). In the presence of *VHL*-KD HK-2 cells (shVHL61 or shVHL25), however, there is a significant increase in the $CD206^+$ population (>20-fold increase) and in the $CD163^+$ population (∼30-fold increase). The *in vitro* assays were repeated using a different human kidney epithelial cell line HEK293 (Supplementary Fig. S2C). The result confirms that THP-1 cells respond to *VHL* inactivation in HEK293 in a similar manner to that in HK-2 (Supplementary Fig. S2D and S2E).

The enrichment of M2 in the presence of *VHL*-deficient cells is verified *in vivo*. As shown in Supplementary Fig. S2F, there are no or very few $CD206^+$, $CD163^+$, or Arginase-1 ($Arg\text{-}1^+$) cells in WT kidneys, and these M2 populations are increased significantly in $Vhlh^{KO}$. In contrast, WT kidney contains a small number of M1 ($CD86^+$) macrophages, and the number is increased but by a comparatively more moderate extent in VHL^{KO} (Supplementary Fig. S2F). In clinical samples, we also observe the general trend of increased

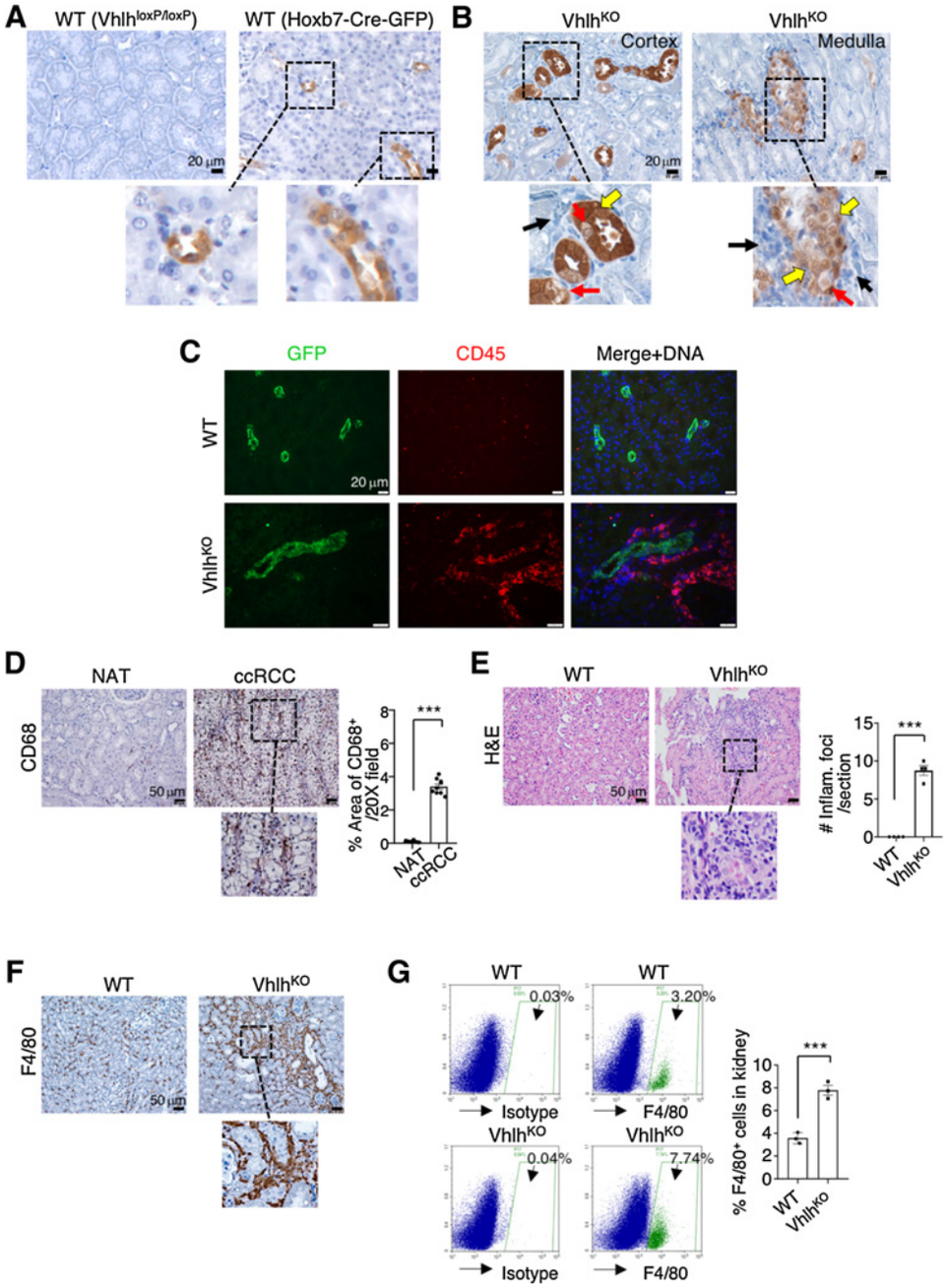

Figure 1.

VHL deficiency generates inflammatory, clear-cell, macrophage activation, and adenoma-like phenotypes. **A** and **B**, Paraffin kidney sections from WT controls (*Vhlh*$^{loxP/loxP}$ or *Hoxb7-Cre-GFP*; **A**) and Vhlh^{KO} (*Hoxb7-Cre-GFP; Vhlh*$^{loxP/loxP}$; **B**) are stained for GFP and counterstained with hematoxylin. *Vhlh*$^{loxP/loxP}$ shows no GFP expression, while *Hoxb7-Cre-GFP* shows GFP expression in morphologically normal kidney tubule cells. In Vhlh^{KO}, there are abnormal GFP^{+} cells that exhibit clear-cell phenotype (red arrows) and multilayering (adenoma; yellow block arrows). There is also an increased number of immune cells (black arrows) in the vicinity of GFP^{+} tubules. Representative images from 4 to 5 animals are shown. **C,** WT and Vhlh^{KO} kidney sections are processed for staining for GFP (green) and CD45 (red). **D,** Representative human grade 1 or grade 2 ccRCC tissues ($n = 8$) including NAT and tumor proper (ccRCC) were stained for the macrophage marker CD68 and counterstained with hematoxylin. The inset shows a significant number of macrophages in the interstitial space in ccRCC. Quantification is shown on the right. Each data point is the average of four 20× fields of view from one sample. **E,** Representative 3-month-old WT and Vhlh^{KO} mouse kidney tissues ($n = 4$) stained with hematoxylin and eosin (H&E). The insets show extensive infiltration of immune cells in areas of the Vhlh^{KO} tissues (inflammatory foci). Scale bars, 50 μm. Quantification is shown on the right. Each data point is the total number of foci in one center section of a kidney from one sample. **F,** Representative 3-month-old WT and Vhlh^{KO} mouse tissues ($n = 4$) stained for the mouse macrophage marker F4/80 and counterstained with hematoxylin. **G,** Representative flow cytometry of mouse whole kidney cell suspensions (devoid of erythrocytes) stained for the mouse macrophage marker F4/80. Quantification of positively stained cells per kidney is shown on the right. Error bars, SEM. ***, $P < 0.001$.

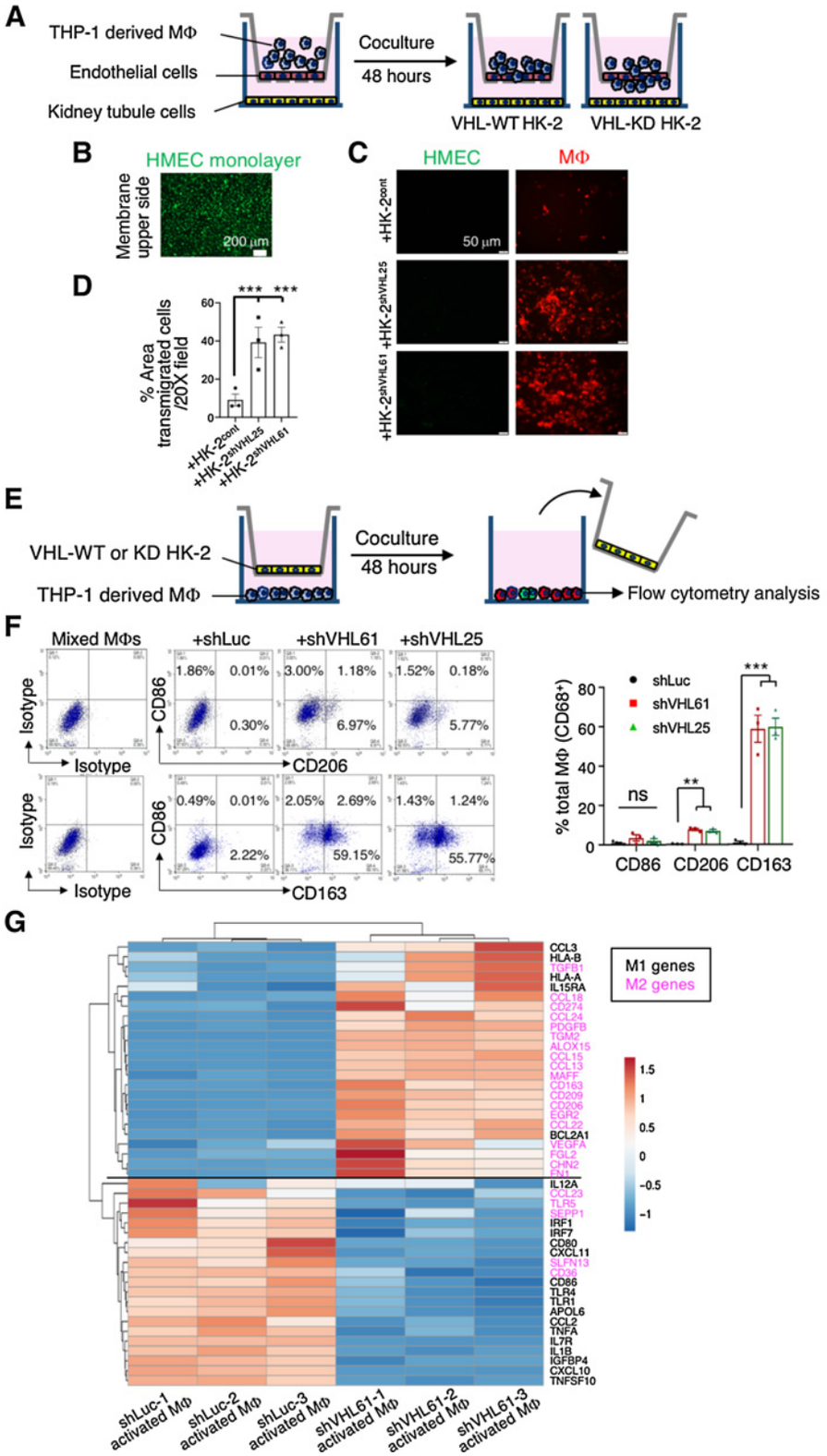

Figure 2.

VHL-deficient kidney tubule cells induce macrophage extravasation and polarization toward the M2 phenotype. **A,** Schematics of the coculture system. **B,** The HMECs labeled with CellTrackerGreen CMFDA Dye were grown to confluency. Scale bar, 200 μm. **C,** The cocultured macrophages (MΦ) labeled with CellTracker Red CMTPX Dye that migrated through the endothelial cell monolayer and the porous membrane to the underside of the membrane are visualized. **D,** Quantification of the extravasated macrophages. Each data point is the average of four 20× fields of view from one experiment. **E,** Schematics of the coculture experiment for assaying induction of macrophage polarization. The membrane pore size of the upper chamber is 0.4 μm so the kidney tubule cells in the upper chamber could not transmigrate to the lower chamber. **F,** Macrophages cocultured with HK-2 cells with or without *VHL* KD were collected, stained using IgG isotype control, or antibodies against human CD86 and CD206, or CD86 and CD163 before being subjected to flow cytometry analysis. Quantification is shown on the right. **G,** Heatmap generated by unsupervised clustering of M1 (black font)- and M2 (pink font)-specific genes in THP-1–derived macrophages cocultured with HK-2 cells with or without *VHL* KD. A summary of the result is shown in Supplementary Table S4. shVHL61 and shLuc are shRNA constructs specific for *VHL* and *luciferase* (as negative control), respectively. Error bars, SEM. **, $P < 0.01$; ***, $P < 0.001$; ns, no significance.

M2-type macrophages in tumors (Supplementary Fig. S3). In the tumor samples, we also included peritumor tissues that are defined as regions abutting the tumor proper. These regions do not contain malignant cancer cells but are usually rich in immune cells and show fibrosis, similar to the phenotypes in our mouse $Vhlh^{KO}$ kidneys. Interestingly, M1-type macrophages ($CD86^+$) are increased in peritumor tissue, and the level is significantly reduced in tumors. With M2-type macrophages, $CD163^+$, $CD206^+$, and ARG-1^+ cells are all significantly increased in peritumor tissue, and early- and advanced-stage tumors. A previous meta-analysis has shown that a higher number of $CD163^+$ TAMs is associated with poor overall survival and progression-free survival (30).

To determine whether the proliferation of resident macrophages can play a role in the increase of macrophage number, we first examined whether *VHL*-deficient epithelial cells could induce macrophage proliferation. The result shows that the levels of Ki-67 positivity do not change in THP-1 cells with or without HK-2 coculture. When cocultured with HK-2, there is also no change in proliferation capacity regardless of the status of *VHL* activity (Supplementary Fig. S4A).

We additionally performed immunofluorescence double staining for Ki-67 and CD81 (a kidney resident macrophage marker; ref. 31) on WT and $Vhlh^{KO}$ kidney sections. The result shows that the $CD81^+$ macrophages do not exhibit proliferation capacity (no Ki-67 coexpression; Supplementary Fig. S4B) and the number of these macrophages does not change with or without *Vhlh* KO (Supplementary Fig. S4C). We, therefore, conclude that the local expansion of resident macrophages does not play a significant role in the overall increase of macrophage number in the *VHL*-deficient tissue.

The increase of M1 and the proportion of induced $CD163^+$/$CD206^+$ M2 populations *in vivo* are somewhat different from the *in vitro* results with human cells. This likely reflects the difference between species or the complexity *in vivo*, although the general trend is consistent with the *in vitro* assay. This notion is demonstrated in Supplementary Fig. S5 using the mouse macrophage cell line RAW264.7 (Supplementary Fig. S5A and S5B) and the peripheral blood–derived primary human $CD14^+$ monocytes (denoted as PBMCs; Supplementary Fig. S5C and S5D).

To further verify the M2 phenotype enrichment suggested by the above analyses, we examined the global gene expression signature of macrophages stimulated by *VHL*-KD HK-2 (HK-2^{VHLKD}) versus control HK-2 (HK-2^{cont}) cells. The THP-1-derived macrophages were cocultured with HK-2 cells with or without *VHL* KD for 48 hours, and the macrophages (in the bottom well of a Boyden chamber) were collected and processed for bulk RNA sequencing (RNA-seq). The RNA-seq results show that, indeed, there is a significant enrichment of M2 genes versus M1 genes (based on previously documented M1–M2 gene set; refs. 32, 33) in HK-2^{VHLKD}-activated macrophages. Among the 24 significantly upregulated macrophage polarization marker genes in HK-2^{VHLKD}-activated macrophages, 19 (79%) are known as M2 markers. Conversely, among the 21 significantly downregulated marker genes, 16 (76%) are known as M1 markers (**Fig. 2G**; Supplementary Table S4). The expression of some of these marker genes is verified (Supplementary Fig. S6).

Collectively, these experiments show that *VHL/Vhlh*-deficient kidney tubule cells not only induce macrophage infiltration but also macrophage polarization preferentially toward the M2 phenotype.

VHL-deficient kidney tubule cells secrete increased levels of IL6

The transwell coculture experiment described above suggests that macrophage extravasation and polarization are induced by soluble factors secreted by the *VHL*-deficient kidney tubule cells. To identify these factors, Bio-Plex Pro Human Cytokine Screening Platform was used to analyze the cytokine/chemokine components in the conditioned media (CM) of HK-2 cells with or without *VHL* KD. Among the 50 cytokines and chemokines included in the array, only one, IL6, shows both high expression level and the most significant enrichment in the CM of *VHL* KD cells compared with control (**Fig. 3A**; Supplementary Table S5). Another enriched factor CXCL1 is expressed at a moderate level and is best known for its chemotactic function for neutrophils (34). Interestingly, other traditionally recognized potent macrophage-activating factors such as MCP-1 (CCL2), MCP-3 (CCL7), IL10, and M-CSF (CSF1) are present at very low levels in the CM with or without *VHL* KD. This indicates that the cytokine program emanating from the *VHL*-deficient cells is specific in its targets and scope. The increase of IL6 in the CM of *VHL* KD HK-2 cells is verified by ELISA (**Fig. 3B**).

IL6 is the representative member of a family of cytokines that play important roles in mediating inflammatory responses in pathophysiologic conditions (35). In order to establish the interactive network in the microenvironment of $Vhlh^{KO}$ kidney tissue, we first sought to verify the source of IL6 *in vivo*. As shown in **Fig. 3C**, double staining for the *Cre* driver reporter GFP and IL6 confirms that IL6 is not expressed in WT kidney and is expressed mainly (∼80%) in the *Vhlh*-mutant tubule cells. In human early-stage ccRCC samples, double staining shows that IL6-expressing cells are indeed mostly (∼90%) $CAIX^+$ [a *VHL* mutant cell marker (36)] ccRCC cells (**Fig. 3D**).

To further analyze the identity of nontubule IL6 expressing cells in *VHL*-deficient tissues, we examined IL6 expression together with markers for macrophages (F4/80 or CD68), kidney pericytes and myofibroblasts (PDGFRβ), endothelial cells (CD34 or CD31), and lymphatic endothelial cells (PDPN), in mouse (Supplementary Fig. S7A) and in human ccRCC samples (Supplementary Fig. S7B). Consistent with our previous finding (21), the other IL6-expressing cells are mainly vascular endothelial cells in the *VHL*/*Vhlh*-deficient microenvironment.

IL6 expression has been known to increase in hypoxic conditions (37). We, therefore, consider whether IL6 overexpression in *VHL*-deficient HK-2 cells is mediated by the accumulation of HIF1α. Treatment of HK-2 cells with the HIF1α inhibitor 17-AAG (an antagonist of HSP90-HIF1α interaction; ref. 38) can reduce the HIF1α protein level (Supplementary Fig. S8A) and downregulate the expression of *IL6* mRNA in *VHL*-deficient HK-2 cells (Supplementary Fig. S8B) as well as secretion of IL6 into the CM (Supplementary Fig. S8C).

For identifying the IL6 target cells *in vivo*, we used double staining for IL6R and mouse or human macrophage markers. As shown in **Fig. 3E**, IL6R is almost exclusively expressed in $F4/80^+$ cells (mouse macrophages) in the $Vhlh^{KO}$ kidney. There is no detectable IL6R expression in WT. In human early-stage ccRCC samples, high levels of IL6R are expressed in $CD68^+$ macrophages (**Fig. 3F**).

We further confirmed the expression of IL6R in macrophages *in vitro* using flow cytometry. The result shows that partially differentiated THP-1 contains ∼50% $IL6R^+$ cells, and the size of this population is not influenced by the *VHL* activity in the tubule cells. In the presence of *VHL* KD tubule cells, these $IL6R^+$ cells polarize to a much greater extent toward M2 ($CD163^+$) than M1 ($CD86^+$; Supplementary Fig. S9). We, therefore, conclude that IL6 emanating from the *VHL/Vhlh*-mutant tubule cells mediates the interaction with the IL6R-expressing macrophages.

The IL6-mediated intercellular interaction is likely an important tumorigenic event as analysis of data from The Cancer Genome Atlas

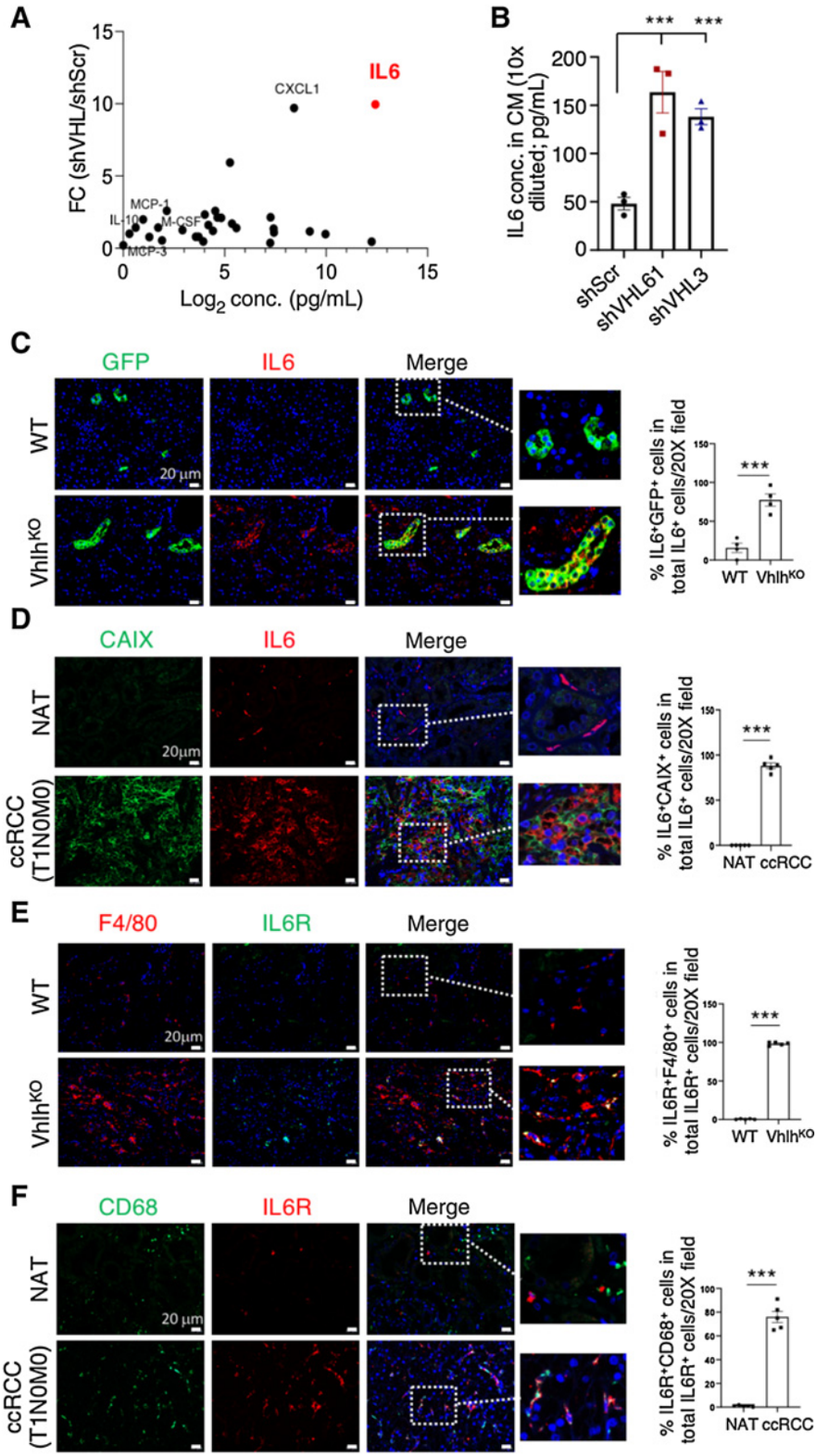

Figure 3.

Increased expression of IL6 signaling components suggests cross-talk between *VHL*/*Vhlh*-deficient kidney cells and macrophages. **A,** CM from HK-2 cells with or without *VHL* KD grown in 10-cm plates were hybridized to the Bio-Plex Pro Human Cytokine Screening Platform. Fold change (FC; shVHL/shScr) versus $\log_2$ concentration in the HK-2-CM is plotted for each cytokine/chemokine, based on quantification data in Supplementary Table S5. **B,** Validation using ELISA quantification of the amount of IL6 in 2 mL of CM of HK-2 cells collected for 24 hours. The final cell number per well was $\sim 0.5 \times 10^6$. The graph shows the CM that was $10\times$ diluted to bring the concentration to the linear range of the assay. **C,** Expression of IL6 in the mouse $Vhlh^{KO}$ kidney is verified by immunofluorescence double staining. GFP marks the *Vhlh* KO cells or the wild-type counterparts. Representative images of four independent animals are shown. **D,** Expression of IL6 in human ccRCC (with the staging of T1N0M0) and the NAT samples were verified by immunofluorescence double staining. CAIX marks the *VHL*-mutant tumor cells. Representative images of five independent sample types; each are shown. **E,** Expression of IL6R in the mouse $Vhlh^{KO}$ kidney was verified by immunofluorescence double staining. F4/80 marks the mouse macrophages. Representative images of four independent animals are shown. **F,** Expression of IL6R in human ccRCC (with the staging of T1N0M0) and the NAT samples were verified by immunofluorescence double staining. CD68 marks the human macrophages. Representative images of five independent sample types; each are shown. Each data point is the average number in four $20\times$ fields of view from one animal. Error bars, SEM. ***, $P < 0.001$.

reveals that high expression levels of IL6 in ccRCC tissues are associated with poor survival (Supplementary Fig. S10A). More interestingly, although in aggregate, IL6 is not highly expressed in low-grade ccRCC compared with normal tissue or high-grade tumors (Supplementary Fig. S10B), in the subpopulation of low-grade tumors (grade 1/2) that does overexpress IL6, the survival rate is significantly lower than that in the low-expressing tumors, which is also true for high-grade tumors (Supplementary Fig. S10C).

IL6 secreted from *VHL*-deficient kidney tubule cells mediates macrophage extravasation and M2 polarization

The cytokine array analysis described above also showed appreciable overexpression of CXCL1 in *VHL*-deficient cells. We therefore first tested the actions of IL6 and CXCL1. To verify their involvement in macrophage infiltration, the *in vitro* extravasation assay described in **Fig. 2A** was repeated in the presence or absence of αIL-6 and/or αCXCL1-neutralizing antibodies. Inactivation of IL6 significantly inhibits macrophage extravasation while inhibiting CXCL1 shows a more modest effect, and the combination of αIL6 and αCXCL1 does not add to the effect of αIL6 alone (Supplementary Fig. S11). The result also shows that αIL6-neutralizing antibody has no effect on the baseline invasiveness of partially differentiated macrophages cocultured with control HK-2 [expressing scrambled shRNA sequence (shScr)]. This suggests that the strong invasive activity of macrophages is induced only in the presence of *VHL*-deficient cells and that autocrine IL6, even if produced by macrophages, has no effect on their baseline invasiveness.

We then tested whether IL6 and CXCL1 are important for M2 polarization (Supplementary Fig. S12). *VHL*-deficient cell-stimulated M2 polarization of THP-1 macrophages can be significantly ameliorated by αIL-6 treatment (Supplementary Fig. S12A and B), but not by αCXCL1 treatment (Supplementary Fig. S12A and C). Furthermore, we could not observe CXCL1 expression in wild-type or *Vhlh* KO kidneys (negative result not shown). In the following analyses, we will therefore focus on the function of IL6.

IL6 inhibition rescues the inflammatory and hyperplastic phenotypes of *Vhlh* KO kidney

To verify the role of IL6 in the development of *Vhlh* KO kidney phenotypes, we injected neutralizing antibody intravenously as an inhibitor of IL6 (**Fig. 4A**). We did not favor the inactivation of *IL6* signaling pathway genes in the *Vhlh* KO background because of unpredictable genetic interaction between *Vhlh* and *IL6* signaling mutations during embryonic development (39, 40). Temporally and spatially specific *IL6* or *IL6R* KO may be attempted but it would require additional *Cre* transgene and/or floxed *IL6/IL6R* constructs. In our experience, such additional genetic manipulations often result in health problems to the animals that may complicate the interpretation of data. On the other hand, αIL6 pathway antibodies have been approved in clinical settings (41, 42). Our experiments could also serve as a proof-of-principle study of αIL6 therapeutics for ccRCC.

Because the *Vhlh* KO phenotypes are fully developed at 3 months of age (20), we began injection of neutralizing antibody (100 μg/mouse) at 2 months of age every week for 4 weeks (**Fig. 4A**). The selection of dosage followed the published protocol (25). We then examined the previously reported *Vhlh* phenotypes (13, 20) such as the appearance of inflammatory foci and hyperplasia. The number of inflammatory foci is greatly increased in $Vhlh^{KO}$ as compared with WT, and the number is significantly reduced upon αIL6 antibody injection in $Vhlh^{KO}$ (**Fig. 4B**). Similarly, the number of hyperplastic ($Ki\text{-}67^{+}$) cells in $Vhlh^{KO}$ mice is also significantly reduced after injection with αIL6 antibody (**Fig. 4C**).

Importantly, the increased number of macrophages in the $Vhlh^{KO}$ kidney is reversed with αIL6 antibody injection (**Fig. 4D**; Supplementary Fig. S13). It is also important to note that αIL6 antibody injection itself does not cause kidney abnormalities or reduction of macrophage number in wild-type mice (**Fig. 4B–D**). The latter observation suggests that IL6 is not required for the maintenance of the kidney tissue-resident macrophages. This is also consistent with the observation (**Fig. 3C**) that WT kidney does not express appreciable levels of IL6. Furthermore, blockade of IL6 produces a significant and specific inhibitory effect on macrophage polarization toward M2. Although the number of $CD86^{+}$ macrophages is unchanged, the number of $CD206^{+}$ or $CD163^{+}$ macrophages is significantly decreased with αIL6 antibody treatment (**Fig. 4D**).

To strengthen the notion that IL6 is the principal regulator of macrophage infiltration and activation, we examined whether the expression of other known macrophage-activation cytokines was altered in the presence of αIL6-neutralizing antibody. As shown in Supplementary Fig. S14, the expression levels of IL4, INFγ, IL10, and M-CSF are increased in the $Vhlh^{KO}$ kidney. However, these cytokines are not expressed by the *Vhlh* KO (GFP^{+}) cells. In particular, IL4 is detected only in areas that are not in the vicinity of GFP^{+} cells. Importantly, their expression levels are not influenced by the αIL6 antibody treatment. This suggests that the action of IL6 on macrophages is not mediated through the known macrophage-activation cytokine signaling.

IL6 signaling–activated macrophages are critical for the development of *Vhlh*-deficient phenotypes

In order to verify the importance of IL6 signaling in macrophage activation, we first generated *IL6R* KD of THP-1 cells (Supplementary Fig. S15A). These *IL6R*-deficient THP-1 cells are impaired in their transendothelial migration in response to stimulation by *VHL*-deficient HK-2 cells (Supplementary Figs. S15B and S15C).

We then tested whether macrophages were important for the *Vhlh* mutant phenotypes *in vivo*. The $Vhlh^{KO}$ and the WT counterparts were treated with clodronate to deplete the endogenous macrophages (Supplementary Fig. S16A and S16B). Importantly, clodronate treatment significantly reduces the inflammatory and proliferative phenotypes of the *Vhlh* KO mouse kidney (Supplementary Fig. S16C and S16D).

Furthermore, when macrophages are reconstituted in clodronate-treated mice using the mouse RAW264.7 cells with or without *IL6R* knockdown (**Fig. 5A**), the phenotypes of inflammation and hyperplasia are restored with the WT RAW264.7 cells (control) but not with the *IL6R*-deficient RAW264.7 cells (**Fig. 5B** and **C**). The reconstitution of macrophages is verified by F4/80 and polarization marker stainings (**Fig. 5D**). Interestingly, infiltration of *IL6R*-KD RAW264.7 into the $Vhlh^{KO}$ kidney is defective, in agreement with the notion that IL6 signaling is required in this process. Inactivation of *IL6R* in the reconstituting macrophages blocks polarization toward M2 but does not affect the M1 population, in a pattern consistent with the result of neutralizing αIL6 antibody treatment described in **Fig. 4D**.

Therefore, specific inhibition of IL6 signaling in $Vhlh^{KO}$ mice can reduce macrophage infiltration and polarization toward M2, which correlates with reduced tissue inflammation and, significantly, proliferation index in the kidney epithelia.

We have shown so far that IL6-mediated macrophage infiltration and polarization play a major role in the development of inflammation-related hyperplasia in tissues containing *VHL/Vhlh*-deficient cells. Nonetheless, the roles of other components in the inflammatory microenvironment cannot be ruled out. We, therefore, examined the

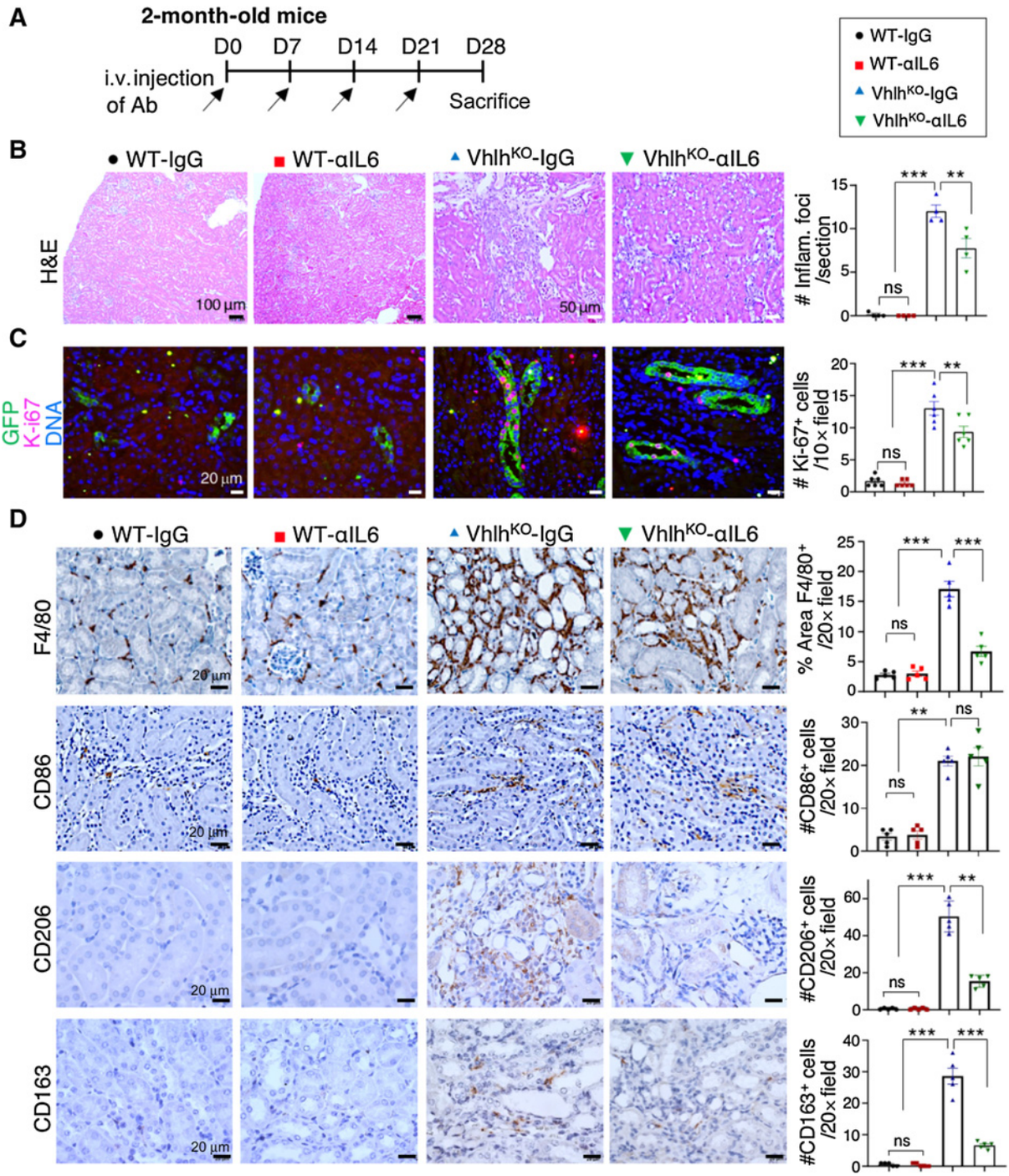

Figure 4.

Inhibition of IL6 rescues *Vhlh* KO phenotypes *in vivo*. **A,** Treatment scheme of 2-month-old mice with αIL6-neutralizing antibody. **B,** Hematoxylin ane eosin (H&E) staining of kidney sections from WT and Vhlh^{KO} mice injected with IgG isotype or αIL6-neutralizing antibody ($n = 4$). Quantification is shown on the right. Each data point is the total number of inflammatory foci in one center section of a kidney from one animal. **C,** Immunofluorescence staining for Ki-67 (pink), GFP (green), and DNA (Hoechst, blue) of kidney sections from WT and Vhlh^{KO} mice injected with IgG isotype or αIL6-neutralizing antibody ($n = 6$). Quantification is shown on the right. Each data point is the average number of Ki-67^{+} cells in four 10× fields of view from one animal. **D,** Characterization of macrophage subsets by IHC staining using macrophage subtype markers in kidney sections after αIL6 antibody treatment ($n = 5$). F4/80 was used as a pan-macrophage marker, CD86 as an M1 marker, and CD206 and CD163 as M2 markers. Quantification is shown on the right. Quantification of F4/80 was done by measuring the positively stained area using ImageJ; each data point is the average of four 20× fields of view in one section from one animal. For the remaining markers, each data point is the average number of positively stained cells of four 20× fields of view in one section from one animal. Error bars, SEM. **, $P < 0.01$; ***, $P < 0.001$; ns, no significance.

expression of makers of representative immune cells: CD4 (regulatory/helper T cells), CD8 (cytotoxic T cells), and $Ly6G^{+}6C^{+}$ (myeloid-derived suppressor cells; MDSC). As shown in Supplementary Fig. S17, T-cell numbers are increased in the $Vhlh^{KO}$ kidney and are decreased upon IL6 inhibition, whereas the MDSC number remains low in all conditions. Therefore, a role for T cells in the development of premalignant ccRCC phenotypes cannot be ruled out. Future studies should integrate their functions when elucidating the complete immune landscape of the ccRCC microenvironment.

Activated macrophages promote mesenchymal phenotypes of the kidney tubule cells

Although cultured ccRCC cell lines such as 786-O exhibit typical mesenchymal characteristics, *VHL* KD in noncancerous HK-2 cells does not cause obvious cell shape change when cultured alone (**Fig. 6A**, top). This indicates that epithelial-to-mesenchymal transition (EMT) is not the direct cell-autonomous effect of *VHL* deficiency but an acquired phenotype of *VHL*-deficient cells brought on via additional mutations or induced by external stimuli. Indeed, influence from the microenvironment has been shown to play an active and critical role in the EMT of cancer cells (43). Interestingly, we noted that $HK\text{-}2^{VHLKD}$ cells, when cocultured with THP-1–derived macrophages, exhibit fibroblast-like cell shape change and a piling-up phenotype, compared with $HK\text{-}2^{cont}$ (**Fig. 6A**, bottom). Cell-shape change is quantified by measuring cell circularity and is shown in **Fig. 6B**.

To understand the role of macrophages in the reciprocal action toward HK-2 cells, we then examined more specifically the activity of macrophages stimulated by HK-2 with or without *VHL* KD. The scheme is depicted in **Fig. 6C**. In this assay, macrophages preincubated with HK-2 cells (with or without *VHL* KD) were then cocultured with fresh HK-2 cells with or without *VHL* KD. Macrophages preincubated with $HK\text{-}2^{cont}$ cells have limited effects on the invasive capacity of either $HK\text{-}2^{cont}$ or $HK\text{-}2^{VHLKD}$ cells (**Fig. 6D**, compare top left with top right plots). In contrast, macrophages preincubated with $HK\text{-}2^{VHLKD}$ cells can promote the invasion of $HK\text{-}2^{cont}$ cells (**Fig. 6D**, compare bottom left with top left plots), and the effect is even more pronounced on $HK\text{-}2^{VHLKD}$ (**Fig. 6D**, compare bottom left with bottom right plots). Quantification of the above result is shown in **Fig. 6E**.

Consistent with these mesenchymal phenotypes, the expression patterns of several EMT markers show a corresponding decrease (E-cadherin) or increase (N-cadherin and vimentin) in $HK\text{-}2^{VHLKD}$ cells stimulated by $HK\text{-}2^{VHLKD}$ cell-activated macrophages (**Fig. 6F** and quantified in Supplementary Fig. S18).

These results indicate that macrophages activated by *VHL*-deficient kidney tubule cells can promote EMT-like phenotypic changes of both wild-type and *VHL*-deficient tubule cells. Importantly, *VHL*-deficient tubule cells can exhibit higher invasive potential than the wild-type counterparts, but this capacity is expressed only with extrinsic stimulation from macrophages that are activated by *VHL*-deficient cells.

CCL18 and TGFβ1 are required for the EMT phenotypes of kidney tubule cells

The M2 markers CCL18 and TGFβ1 have been implicated in TAM-induced tumor EMT (44, 45). Among the inflammation-generated EMT inducers compiled previously (43, 46), *CCL18* is highly enriched in $HK\text{-}2^{VHLKD}$-stimulated macrophages, as identified by our comparative transcriptomes (**Fig. 7A**). *TGFβ1*, the well-known inducer of EMT, is also overexpressed by the activated macrophages, albeit to a lesser extent (**Fig. 7A**). *CCL20* and *VEGFA* are also upregulated but expressed at lower levels. Other inflammation-related EMT inducers such as *WNT, IL6, HGF, EGF*, etc., are not expressed at appreciable levels in either $HK\text{-}2^{cont}$- or $HK\text{-}2^{VHLKD}$-cocultured macrophages, and many other known inflammation-related EMT inducers are in fact downregulated (**Fig. 7A**).

Two other highly enriched chemokine genes *CCL22* and *CCL13* in the transcriptome of macrophages activated by *VHL*-deficient HK-2 cells (Supplementary Table S4) show no increases in secreted protein levels in the CM (Supplementary Fig. S19).

To further confirm the overexpression of CCL18 and TGFβ1 by activated macrophages, we quantified their presence in the CM of HK-2–activated macrophages by ELISA. There is indeed a significant increase of CCL18 and TGFβ1 in the CM of macrophages activated by $HK\text{-}2^{VHLKD}$ cells compared with $HK\text{-}2^{cont}$ (**Fig. 7B**). Because macrophage activation by *VHL*-deficient cells is likely mediated by IL6 signaling, we tested whether IL6 signaling is responsible for CCL18 and TGFβ1 upregulation. As shown in Supplementary Fig. S20, either p-STAT3 (IL6 signaling mediator) inhibitor C188-9 (Supplementary Fig. S20A) or neutralizing αIL-6R antibody (Supplementary Fig. S20B) treatment can inhibit TGFβ1 and CCL18 levels in the CM of either human $CD14^{+}$ PBMCs or THP-1 cells stimulated by *VHL*-deficient HK-2 cells.

The function of CCL18 and TGFβ1 was then tested by repeating the coculture experiments described in **Fig. 6A** with the inclusion of neutralizing anti-CCL18 and/or anti-TGFβ (αCCL18 and/or αTGFβ) antibodies in the CM (45, 47).

In the presence of neutralizing αCCL18 and/or αTGFβ antibodies, the $HK\text{-}2^{VHLKD}$ cells cocultured with macrophages reverted from elongated shape to the typical epithelial cell shape (**Fig. 7C**). The chemotactic invasiveness of HK-2 cells induced by cocultured macrophages is also reduced by neutralizing αCCL18 and/or αTGFβ antibodies (**Fig. 7D**). Furthermore, αCCL18 and αTGFβ can restore E-cadherin expression while reducing the expression of N-cadherin and vimentin in the cocultured *VHL* KD HK-2 cells (**Fig. 7E**; and quantified in Supplementary Fig. S21).

These results suggest that the production of CCL18 and TGFβ1 from the activated macrophages can induce mesenchymal phenotypes of the *VHL*-deficient tubule cells, thus forming a reciprocal activation signaling system between the epithelial tumor cells and the immune component macrophages.

In vivo, the EMT marker N-cadherin and β-catenin are overexpressed in the *Vhlh*-mutant tubule cells compared with wild-type cells (**Fig. 7F**, top and middle), and the increase is ameliorated with αIL6 antibody treatment. Because CCL18 has no equivalent in mice, we only verify that TGFβ is overexpressed by macrophages in the *Vhlh* KO kidney (**Fig. 7F**, bottom). Importantly, the overexpression of TGFβ in mutant-associated macrophages is reduced to background levels with αIL6 antibody treatment. It is worth noting that, despite high levels of N-cadherin and β-catenin expression in *Vhlh* mutant (GFP^{+}) cells in the abnormal tubules, mesenchymal *Vhlh*-mutant (GFP^{+}) cells have not been clearly identified in the interstitial space. Therefore *in vivo*, the EMT phenotype is not necessarily equivalent to cells breaking away from the epithelia. Instead, the EMT characteristics defined by marker gene expression may be an indication of altered epithelial integrity that leads to adenoma-like phenotype (**Fig. 1B**). This may also explain that expression of fully mesenchymal cell markers such as vimentin and αSMA is not detected in *Vhlh*-mutant cells (negative result not shown).

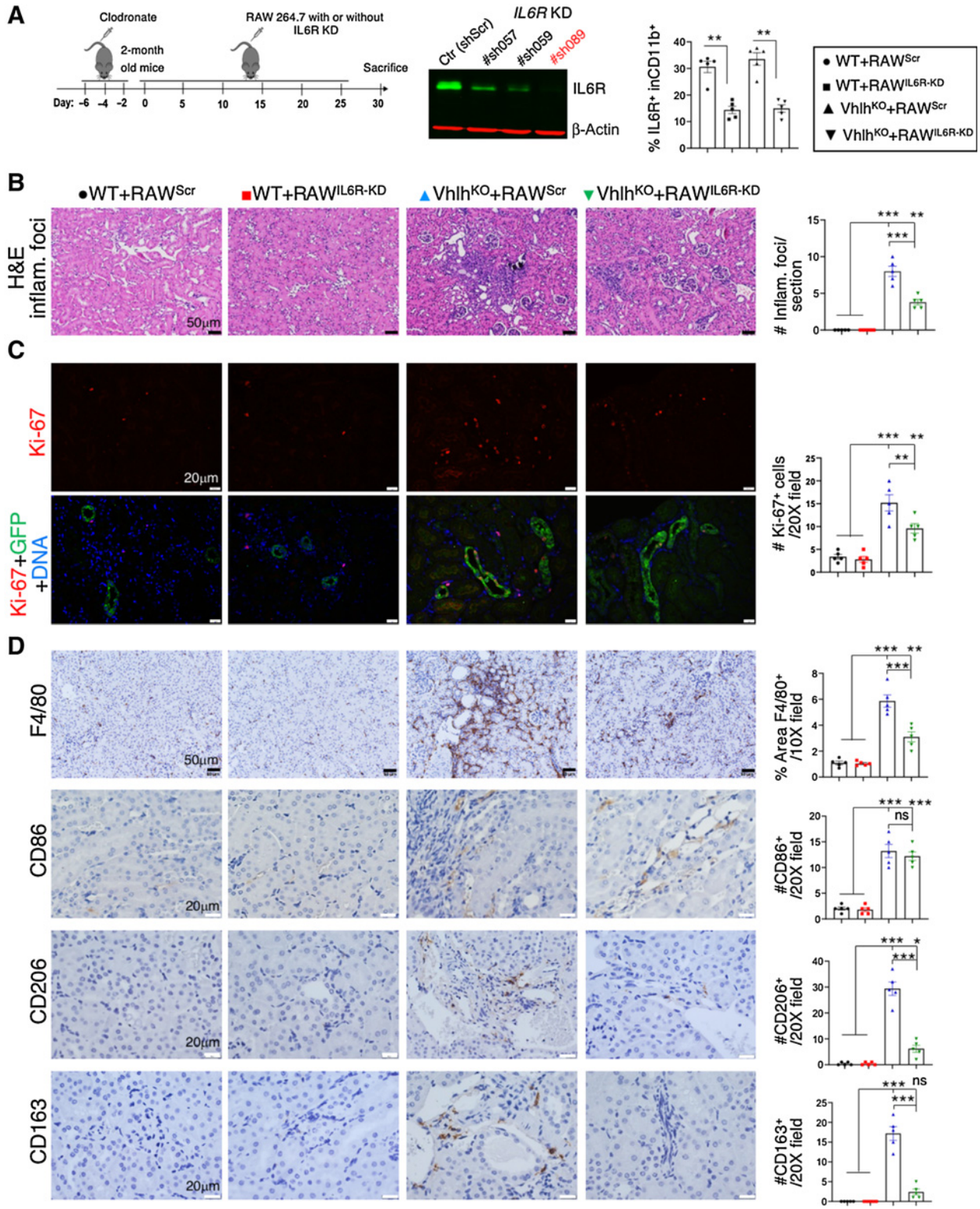

Figure 5.

IL6 signaling in macrophages is important for the expression of *Vhlh*-mutant kidney phenotypes. **A,** Left, schematic of 2-month-old mice (WT and Vhlh^{KO}) treated with clodronate and reconstituted with mouse RAW264.7 macrophages with or without *IL6R* knockdown. Middle, the IL*6R* knockdown efficiency of different RAW264.7 lines. #sh089 (red) was used in the *in vivo* experiment. Right, percentage of IL6R^{+} cells in all CD11b^{+} cells obtained from peripheral blood of the mouse strains as indicated. The KD efficiency remains at >50% *in vivo*. (*Continued on the following page.*)

CCL18-expressing macrophages promote tumor growth and metastasis of ccRCC cells *in vivo*

As CCL18 is not present in mice, to test its oncogenic function, we turn to a modified xenograft model. Also, as TGFβ is highly pleiotropic and a tumor suppressor for early-stage tumors (48), its usefulness as a tumor therapeutic target is uncertain. We, therefore, focus on the action of CCL18 in the progression of human ccRCC. To test whether CCL18-expressing macrophages play a role in ccRCC progression, an orthologous xenograft model combined with exogenous macrophage transplantation was designed to specifically test the oncogenic activity of TAMs. The experimental design is illustrated in Supplementary Fig. S22A. As we intend to test whether CCL18 promotes EMT and metastasis, our *Vhlh* KO model that produced only benign tumor does not serve the purpose. The ccRCC cell line 786-O (expressing luciferase) was therefore used. We tested whether the system could approximate the endogenous ccRCC growth by replacing the mouse macrophages with the human primary $CD14^+$ PBMCs.

As a control, we determined that the number of $F4/80^+$ cells in the kidney was reduced 5- to 6-fold two days after the completion of clodronate treatment, and the level of endogenous mouse macrophages remained low at 7 days after clodronate treatment (Supplementary Fig. S22B). 786-O alone or 786-O + PBMCs cell mixture was injected under the renal capsule of these mice two days after the completion of clodronate pretreatment. Booster i.v. injections of PBMCs (1×10^6 cells/100 μL) were performed at 7, 14, and 21 days after tumor implantation. The growth of the primary tumor was monitored by the Spectrum *In Vitro* Imaging System (IVIS; Supplementary Fig. S22C). The result shows that exogenous human primary PBMCs significantly increase the growth of 786-O. Local invasiveness is also significantly increased in the presence of PBMCs (Supplementary Fig. S22D).

The presence of exogenous PBMC-derived macrophages within the primary tumor is verified by the detection of human $CD68^+$ cells. There is indeed a substantial accumulation of $CD68^+$ cells in the xenografted tumor proper whereas no $CD68^+$ signal is detected in the 786-O only sample (Supplementary Fig. S22D and S22Ea). In addition, human PBMCs can significantly increase the vascular density ($CD34^+$) in the primary tumor, as compared with 786-O only (Supplementary Fig. S22D and S22Eb).

Most importantly, as shown in Supplementary Fig. S22F, PBMCs can increase metastatic tumor growth of 786-O to lung (5/5 with PBMCs vs. 0/5 without PBMCs) at 5 weeks. IHC for 786-O cells shows that, although there are a number of single-cell micrometastases in both 786-O only and in 786-O + PBMCs, only 786-O + PBMCs can generate a high number of metastasis foci of more than 10 cells in size. These phenotypes are consistent with the observation that proliferation index (Ki-67 expression) and EMT marker expression are also increased in the primary tumor mixed with PBMCs (Supplementary Fig. S23).

We further tested more specifically the function of CCL18 in macrophages. The clodronate treatment and the 786-O xenograft were performed with the use of human monocyte THP-1 expressing either scrambled shRNA ($THP\text{-}1^{Scr}$) or *CCL18*-specific shRNA ($THP\text{-}1^{CCL18KD}$; **Fig. 8A**). The efficacy of *CCL18* KD was tested (Supplementary Fig. S24A) and the $THP\text{-}1^{CCL18KD}$ strain showing the most efficient *CCL18* KD was validated for its reduced CCL18 secretion into CM after stimulation with *VHL* KD HK-2 cells (Supplementary Fig. S24B). Of note, this strain of *CCL18*-KD THP-1 cells does not show altered cell shape or growth characteristics. The growth of xenografted primary tumor was monitored by IVIS (**Fig. 8B**). The result shows that exogenous macrophages (THP-1) can significantly increase the growth of 786-O, and this capability is significantly reduced when *CCL18* is knocked down in the THP-1. The extent of local invasiveness is significantly increased in the presence of exogenous THP-1 and is greatly reduced when *CCL18* is knocked down in THP-1 (**Fig. 8C**).

The presence of exogenous THP-1–derived macrophages within the primary tumor was verified by the detection of human $CD68^+$ cells. There is indeed substantial accumulation in the xenografted tumor proper. Interestingly, there is no difference in the number of control THP-1 or THP-1 with *CCL18* KD (**Fig. 8C** and **D** top), indicating that loss of *CCL18* does not affect the viability or infiltration of the exogenous macrophages. As with PBMCs, wild-type THP-1 can significantly increase the vascular density ($CD34^+$) in the primary tumor, and furthermore, *CCL18* KD in THP-1 reduces this capacity significantly (**Figs. 8C** and **D** bottom). This indicates that CCL18 may also contribute to tumor growth via angiogenesis. This is in agreement with the expression of Ki-67 within the primary tumor (Supplementary Fig. S25A). As well, EMT markers such as N-cadherin, β-catenin, and vimentin are increased with the addition of THP-1 in a CCL18-dependent manner (Supplementary Fig. S25B–S25D). Most importantly, as shown in **Fig. 8E**, although there are single-cell micrometastases in 786-O without added macrophages, only 786-O + $THP\text{-}1^{Scr}$ can generate a high number of metastasis foci of more than 10 cells in size, and this capacity is significantly reduced with *CCL18* KD in THP-1 (**Fig. 8E**).

Discussion

In this report, we describe a reciprocal signaling mechanism between the epithelial cells defective in the *VHL* tumor suppressor gene function and macrophages and show that this mechanism is important for the progression of ccRCC. We demonstrate that *VHL*/*Vhlh*-deficient kidney cells can induce macrophage infiltration and polarization toward the traditionally defined protumorigenic M2 phenotype *in vitro* and *in vivo* (**Figs. 1** and **2**; Supplementary Fig. S2; Supplementary Table S4). Because *VHL* deficiency is the driver of a majority of ccRCC (5–7), we believe that inflammatory signal emanating from the premalignant *VHL*-deficient cells should be one of the earliest pathologic events leading to the formation of ccRCC.

We screened for the cytokines and chemokines preferentially secreted by the *VHL*-deficient kidney tubule cells. The most abundant and relevant is IL6 (**Fig. 3A** and **B**). It is worth noting that other

(*Continued.*) **B,** Hematoxylin and eosin (H&E) staining of kidney sections from WT and $Vhlh^{KO}$ mice reconstituted with RAW264.7 cells with or without *IL6R* KD. Quantification of the number of inflammatory foci is shown on the right. Each data point is the total number of inflammatory foci in one center section of a kidney from one animal. **C,** Immunofluorescence staining for Ki-67 (red), GFP (green), and DNA (Hoechst, blue) of kidney sections from WT and $Vhlh^{KO}$ mice treated as above ($n = 5$). Quantification is shown on the right. Each data point is the average number of $Ki\text{-}67^+$ cells in four 20× fields of view from one animal. **D,** Characterization of macrophage subsets by IHC staining using macrophage subtype markers in kidney sections of mice treated as above. F4/80 was used as a pan-macrophage marker, CD86 as an M1 marker, and CD206 and CD163 as M2 markers. Quantification is shown on the right. Quantification was done by measuring the area stained with F4/80 using ImageJ. Each data point is the average of four 10× fields of view in one section from one animal. For the remaining markers, each data point is the average number of positively stained cells of four 20× fields of view in one section from one animal. $n = 5$. Error bars, SEM. **, $P < 0.01$; ***, $P < 0.001$; ns, no significance.

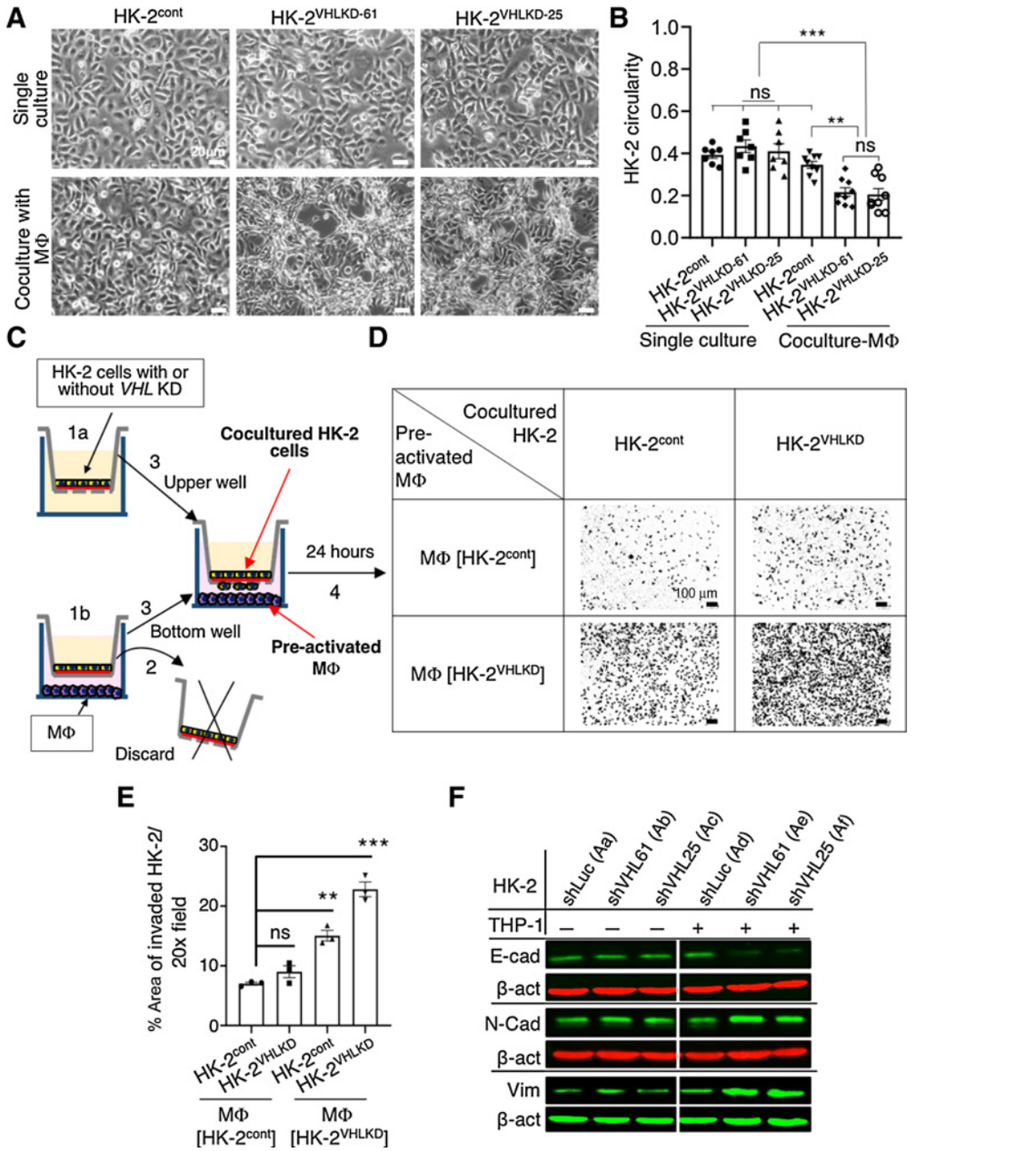

Figure 6.

Activated macrophages promote EMT phenotypes in kidney tubule cells. **A,** HK-2 cells with or without *VHL* KD are cultured alone (top) or cocultured with partially differentiated THP-1 (bottom). Forty-eight hours later, HK-2 cells were observed under a light microscope and quantified for the cell shape change. **B,** Cell shape change observed in **A** was quantified by cell circularity using ImageJ software, which was defined as the shorter of the two diameters of a cell divided by the longer diameter. Each data point is the average of 6 random cells and 7 to 9 data points were collected for each sample. **C,** Schematic of the kidney cell invasion assay. 1a, HK-2 cells with or without *VHL* KD are cultured alone in the upper well (with 8-μm pores) of the Boyden chamber coated with Matrigel and allowed to grow to ∼60% confluency. 1b, Meanwhile another portion of HK-2 cells with or without *VHL* KD are plated in the upper well (with 0.4-μm pores) and cocultured with partially differentiated THP-1 in the bottom well in the presence of minimal media. 2, Forty-eight hours later, the upper well containing the HK-2 cells in the coculture 1b, is discarded. 3, The HK-2 monoculture in the other upper well (1a) is then placed over the activated macrophages in 1b. 4, Twenty-four hours later, the invasiveness of the HK-2 cells through the upper well membrane is quantified after staining with crystal violet. **D,** Control (with shLuc) or *VHL* KD (with shVHL61) HK-2 cells (HK-2^{cont} or HK-2^{VHLKD}, respectively) exhibit similar invasiveness in the presence of HK-2^{cont}-cocultured macrophages (top), whereas the invasive capacity of HK-2^{cont} is significantly induced in the presence of HK-2^{VHLKD}-activated macrophages (compare bottom left with top left plots). The invasive capacity is even more pronounced with HK-2^{VHLKD} induced by HK-2^{VHLKD}-activated macrophages (compare bottom right with bottom left plots). **E,** Quantification of the results in **D**. Each data point is the average of four 20× fields of view from one experiment. **F,** EMT marker gene expression in HK-2 cells with or without *VHL* KD cocultured with partially differentiated THP-1. Representative images of three independent experiments are shown. The blot for E-cadherin is stripped and rehybridized for N-cadherin. Uncropped Western blots and quantification are shown in Supplementary Fig. S18. Error bars, SEM. **, $P < 0.01$; ***, $P < 0.001$; ns, no significance.

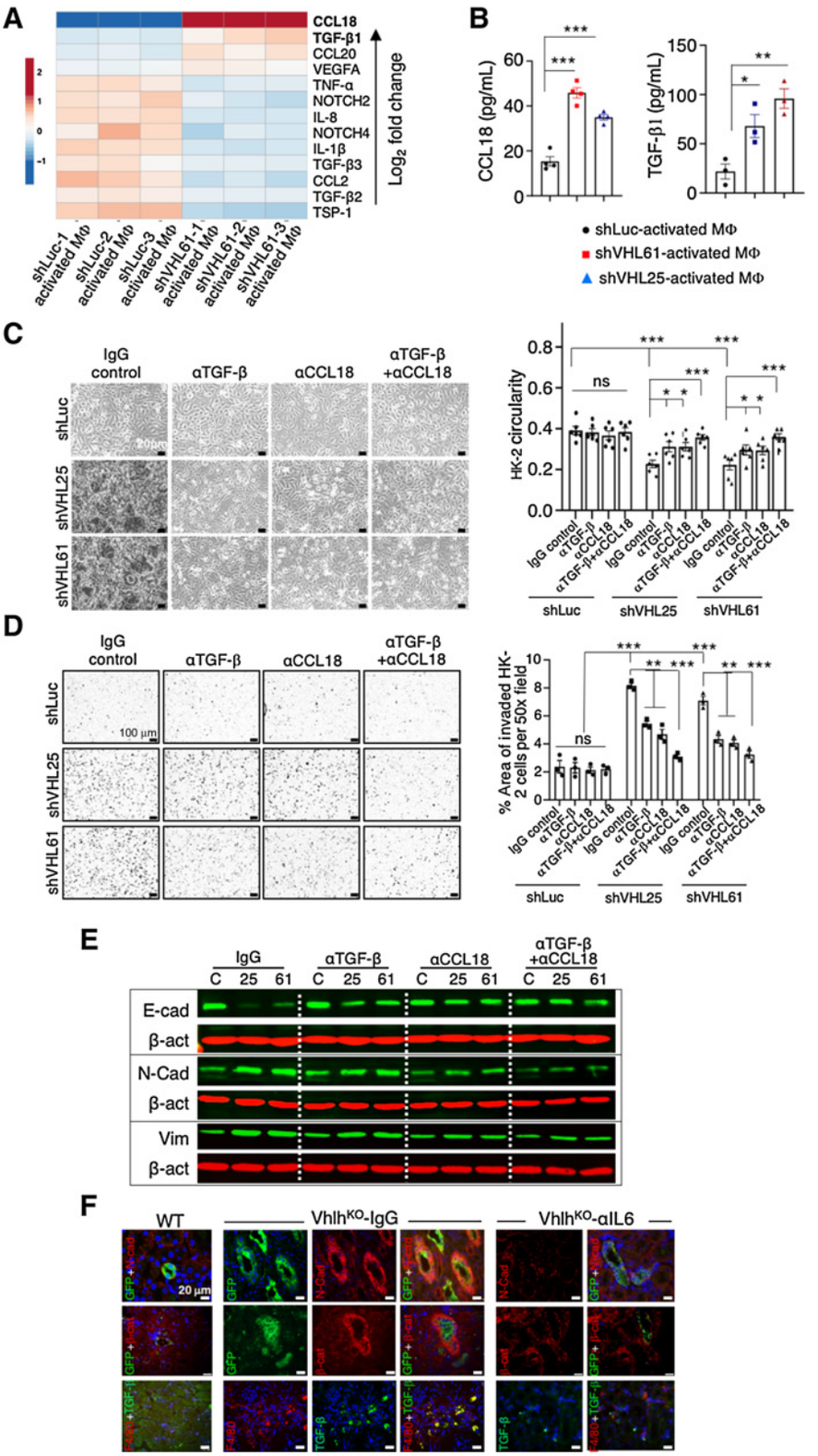

Figure 7.

Macrophage-induced EMT phenotypes in HK-2 cells are dependent on CCL18 and TGFβ1. **A,** Heatmap of EMT-inducer gene expression (based on transcriptome generated by RNA-seq) comparing macrophages cocultured with HK-2 cell with (shVHL61) or without (shLuc) *VHL* KD. Clustering is based on $\log_2$-fold change (shVHL61/shLuc). **B,** Partially differentiated THP-1 cocultured with HK-2 cells with or without *VHL* KD for 2 days in 12-well Boyden chambers (with 0.4-μm pores) were then grown without HK-2 cells in 0.7 mL minimal media for 24 hours. The final cell number per well is $\sim 0.2 \times 10^6$. The CM were quantified for the levels of CCL18 and TGFβ1 without dilution using ELISA. **C,** Coculture of HK-2 cells with or without *VHL* KD and partially differentiated THP-1 was performed as in **Fig. 6A**, with the addition of IgG isotype into the media, or αCCL18 and/or αTGFβ neutralizing antibodies at 10 μg/mL and 30 μg/mL, respectively. Right, quantification of the results, expressed as cell circularity as described in **Fig. 6B**. Macrophage-induced cell shape change in HK-2 cells was reversed with treatment of αCCL18 and/or αTGFβ. **D,** Coculture of HK-2 cells with or without *VHL* KD and partially differentiated THP-1 was performed as in **Fig. 6C**, with the addition of IgG isotype, or αCCL18 and/or αTGFβ-neutralizing antibodies into the media. Representative images of three independent experiments are shown. The invasiveness of the HK-2 cells is quantified on the right. Each data point is the average of three 20× fields of view measuring the percentage of coverage by the migrated cells. **E,** Coculture of HK-2 cells with or without *VHL* KD [25 and 61, or C (control), respectively] with partially differentiated THP-1 was performed as in **Fig. 6A**, with the addition of IgG isotype, or αCCL18 and/or αTGFβ-neutralizing antibodies into the media. The HK-2 cells were collected and processed for Western blot analysis with indicated antibodies. Representative images of three independent experiments are shown. Uncropped Western blots and quantification are shown in Supplementary Fig. S21. **F,** Top and middle, kidney sections of WT and Vhlh^{KO} mice injected with IgG isotype or αIL6 antibody were stained for GFP (green), N-cadherin (N-cad; red; top), or β-catenin (β-cat; red; middle), and DNA (Hoechst, blue). Representative images of three independent samples are shown. Bottom, kidney sections as above were stained for F4/80 (red), TGFβ (green), and DNA (Hoechst, blue). Representative images of three independent samples are shown. Error bars, SEM. *, $P < 0.05$; **, $P < 0.01$; ***, $P < 0.001$; ns, no significance.

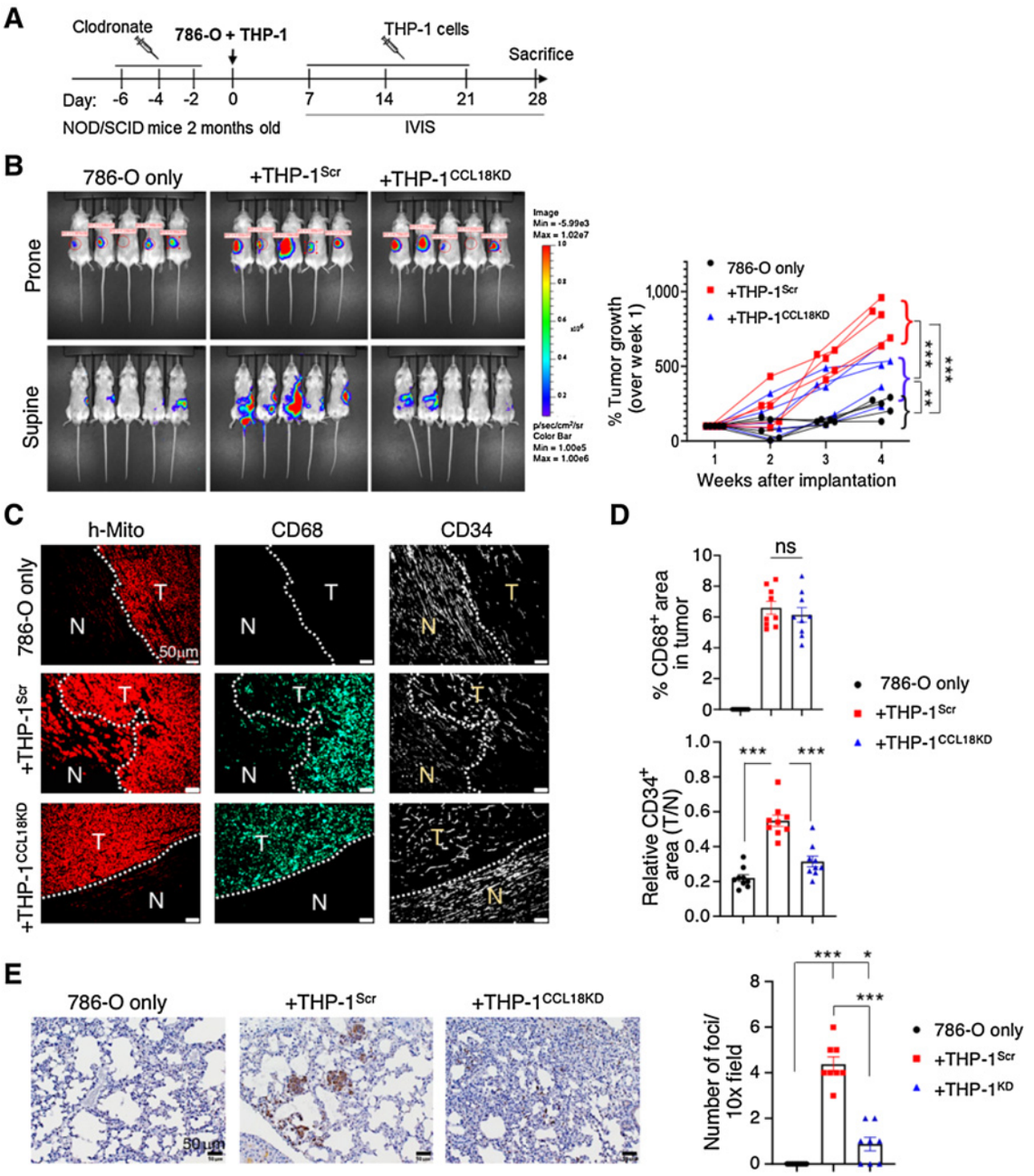

Figure 8.

CCL18-expressing macrophages promote ccRCC tumor growth and metastasis. **A,** A total of 5×10^5/10 μL of 786-O ccRCC cells expressing luciferase were used alone or 4.5×10^5/10 μL were mixed with 0.5×10^5 human monocyte THP-1 expressing either scrambled shRNA (THP-1^{Scr}) or *CCL18*-specific shRNA (THP-1^{CCL18KD}). The mixture was injected under the renal capsule of NOD/SCID mice pretreated with 1 mg/0.2 mL every other day of chlodronate-embedded liposomes for 6 days. Booster i.v. injections with THP-1 (1×10^6/100 μL) were performed at 7, 14, and 21 days after tumor implantation. **B,** IVIS analysis of representative (from a total of 9) xenografted mice at 4 weeks after implantation in prone and supine positions. Quantification of tumor growth through 4 weeks is shown on the right. **C,** Kidneys containing primary tumors were stained for 786-O (human mitochondrial marker; h-Mito), vasculature (mouse CD34), and human macrophages (CD68). The extent of local invasiveness was increased with exogenous THP-1 but reduced when *CCL18* was knocked down in THP-1. The presence of macrophages derived from THP-1 was validated by staining for human CD68. The extent of tumor-associated angiogenesis was assessed by staining for CD34. Note that because of secondary antibody compatibility, the more common endothelial marker CD31 was not used. N, normal tissue; T, tumor. **D,** Top, quantification of the CD68$^+$ signal in tumor vs. normal tissue shown in **C**. Bottom, quantification of the CD34$^+$ signal in tumor vs. normal tissue shown in **C**. **E,** Lung tissue sections at 4 weeks after transplantation were stained for human mitochondria. Quantification of the number of metastasis foci ≥20 μm (~10 cells) is shown on the right. The data are presented as mean ± SEM. *, $P < 0.05$; **, $P < 0.01$; ***, $P < 0.001$; ns, no significance.

traditionally recognized potent macrophage-activating factors such as MCP-1/CCL2, MCP-3/CCL7, IL10, and CSF1/M-CSF are expressed at very low levels with or without *VHL* KD (**Fig. 3A**; Supplementary Table S5). This indicates that *VHL*-deficient cells express a specific regulatory program to communicate with macrophages. This program may be related to the finding that IL6 expression can be induced by hypoxic (or in the case of *VHL* deficiency, pseudohypoxic) conditions (37). This program is verified in mouse kidney tissue, because IL6 is expressed in the *Vhlh* KO kidney cells but not in wild-type (**Fig. 3C**), and IL6R is expressed in the macrophages in *Vhlh* KO kidney but not in WT kidney (**Fig. 3E**), although trans-signaling of IL6 through soluble IL6R, which can potentially target other cell types, cannot be formally ruled out (49). In the case of human ccRCC samples, expression of IL6 is detected in early-stage ccRCC but not in NAT (**Fig. 3D**), and IL6R is expressed in TAMs but not in NAT (**Fig. 3F**). This also indicates that the IL6-induced macrophage activation occurs at the premalignant stage of ccRCC progression. The importance of IL6 signaling is verified *in vivo* by rescuing $Vhlh^{KO}$ mouse phenotypes with αIL6-neutralizing antibody treatment (**Fig. 4**). Furthermore, depletion of endogenous macrophages can reduce $Vhlh^{KO}$ mouse phenotypes (Supplementary Fig. S16) and the phenotypes can be restored by reconstituting with exogenous macrophages in an IL6R-dependent manner (**Fig. 5**).

When cocultured with macrophages, the *VHL*-deficient kidney cells exhibit features of EMT (**Fig. 6**; Supplementary Fig. S18). Interestingly, the cell-autonomous effect of *VHL* deficiency can confer increased EMT potential but only in the presence of extrinsic stimuli provided by activated macrophages, reaffirming the importance of stromal interaction in tumor progression. Furthermore, macrophage-secreted CCL18 and TGFβ1 are identified as inducers of EMT phenotypes in *VHL*-deficient tubule cells (**Fig. 7**; Supplementary Fig. S21).

Consistent with the above observations, blockade of IL6 in *Vhlh* KO mice can reduce inflammation and hyperplasia *in vivo* (**Fig. 4B** and **C**). Significantly, exogenous human primary PBMCs and monocyte cell line THP-1 can both greatly enhance the growth and metastasis of ccRCC cells 786-O in xenografted NOD/SCID mice depleted of endogenous macrophages (Supplementary Figs. S22, S23, and S25; **Fig. 8**); and this oncogenic capacity is ameliorated when the *CCL18* gene is knocked down in the THP-1 cells (**Fig. 8**; Supplementary Fig. S25).

These findings support a mechanism by which tissue inflammation is induced by premalignant cells, and the inflammatory microenvironment reciprocally promotes tumor progression via secretion of oncogenic factors. Although IL6 signaling is a well-known cytokine and is a recognized therapeutic target, our study uncovered an important signaling mechanism that places the action of IL6 in tissue context and identified downstream signaling mediated by additional molecules such as CCL18. Interestingly, in our human ccRCC xenograft model, CCL18-expressing macrophages are critical for both tumor growth and metastasis.

We should note that *VHL/Vhlh*-deficient cells can also interact with and activate other components in the microenvironment such as endothelial cells, as we have shown recently (21). Our result also shows that the numbers of both $CD4^+$ and $CD8^+$ T cells are increased in *Vhlh* KO kidney; therefore, their roles in the development of ccRCC phenotypes cannot be ruled out. This does not diminish the importance of IL6 signaling and the activated macrophages, however, as different components in the microenvironment can promote different aspects of tumor progression. For example, although activated ECs can facilitate intravasation and extravasation, it does not appear to promote EMT of the tumor cells (21). The presence of both $CD4^+$ and $CD8^+$ T cells may be critical in fine-tuning between tumor-fighting function and immune tolerance by the host, which warrants detailed future studies.

Accumulated data have indicated that TAMs in RCC show mixed M1/M2 phenotypes as traditionally defined (50). However, in a study involving 185 RCC patients, it was demonstrated that low M1-positive macrophage content and high M2-positive macrophage content were the most important factors associated with reduced survival (51). As such, targeting M2/TAMs has emerged as an attractive strategy for the therapeutic intervention for cancer (15, 16). Although the direct elimination of a specific population of macrophages represents a potential therapeutic strategy, it may be more amenable to target the upstream signaling event that induces the tumorigenic macrophage function. In this sense, our results suggest that IL6 signaling can be a candidate target. Alternatively, CCL18 may be another target that confers the oncogenic function of TAMs. Importantly, the αIL6 antibody treatment did not reduce the level of M1 ($CD86^+$) macrophages (**Fig. 4D**) in our *Vhlh* KO model, suggesting that the population of potential anti-tumor macrophages is preserved in the microenvironment.

IL6 is a potent modulator of macrophage function and has been linked to tumor development, including ccRCC (35, 42). However, its role in inducing tumor cell proliferation and invasion has been in many cases described as an autocrine or intracrine action of the tumor cells (37, 52, 53). This may be the result of studies performed using *in vitro* monoculture of cancer cell lines or tumor explants. Our results reported in this study clearly demonstrate the importance of tissue context, and as a result, the pathophysiologic function of IL6 may be different depending on the contexts. Therapeutics based on inhibition of IL6 signaling has been in a clinical trial as a cancer treatment with mixed results (35, 42). This may be partly because the exact roles of IL6 in tumor progression have not been elucidated clearly, and thus the intended targets and the timing of treatment have not been optimal. It is possible that, as suggested by our results, anti-IL6 signaling therapy should be more suited for premalignant tumors. Indeed the survival rate is significantly lower in a subgroup of ccRCC patients who show increased expression of IL6 at early stages of the disease (Supplementary Fig. S10C).

The results presented here strongly suggest that the action of IL6 in tumorigenesis can be as early as the initiation of tumor formation. Therefore, it is likely that αIL6 therapy may be effective in treating early-stage cancers, or as a preventive therapy for high-risk groups such as familial VHL disease or chronic kidney disease patients. Late-stage tumors may have acquired too many adaptive or alternative malignancy pathways; therefore, simple αIL6 therapy may be insufficient.

In conclusion, in this report, we have outlined a specific mechanism of cross-talk between the fledgling tumor cells and the immune components of the microenvironment, with implications for the initiation and progression of ccRCC (Graphic Abstract). This mechanism can serve as a template for future studies that should include additional components in the microenvironment. Such understanding should change our concept of cancer therapies from killing malignant cells to modulating the microenvironment and early intervention.

Authors' Disclosures

T. Hsu reports grants from the National Health Research Institute, Taiwan, ROC, the Ministry of Science and Technology, Taiwan, ROC, and Taiwan Bio-development Foundation during the conduct of the study. No disclosures were reported by the other authors.

Authors' Contributions

T.-N. Nguyen: Conceptualization, data curation, formal analysis, validation, investigation, visualization, methodology, writing–original draft, writing–review and editing. **H.-H. Nguyen-Tran:** Data curation, formal analysis, investigation, methodology. **C.-Y. Chen:** Data curation, methodology. **T. Hsu:** Conceptualization, resources, data curation, formal analysis, supervision, funding acquisition, validation, investigation, visualization, methodology, project administration, writing–review and editing.

Acknowledgments

This study was supported by a grant from the National Health Research Institute, Taiwan, ROC (#NHRI-EX108-10801BI) and a grant from the Ministry of Science and Technology, Taiwan, ROC (#MOST 109-2320-B-008-002-MY3). The Hsu laboratory is also supported by a Chair Professorship of the Taiwan Biodevelopment Foundation. The authors thank the Molecular and Genetic Imaging Center, National Yang-Ming University, Taiwan Animal Consortium, and Center for Advanced Molecular Imaging and Translation, Chang Gung Memorial Hospital, Linkou, Taiwan, for technical support in IVIS experiments. They are also indebted to the assistance in storage and rederivation of our mouse stock from Taiwan Animal Consortium.

The publication costs of this article were defrayed in part by the payment of publication fees. Therefore, and solely to indicate this fact, this article is hereby marked "advertisement" in accordance with 18 USC section 1734.

Note

Supplementary data for this article are available at Cancer Research Online (http://cancerres.aacrjournals.org/).

Received November 3, 2021; revised April 18, 2022; accepted May 25, 2022; published first June 6, 2022.

References

1. Ljungberg B, Campbell SC, Choi HY, Jacqmin D, Lee JE, Weikert S, et al. The epidemiology of renal cell carcinoma. Eur Urol 2011;60:615–21.
2. Hsieh JJ, Purdue MP, Signoretti S, Swanton C, Albiges L, Schmidinger M, et al. Renal cell carcinoma. Nat Rev Dis Primers 2017;3:17009.
3. Makhov P, Joshi S, Ghatalia P, Kutikov A, Uzzo RG, Kolenko VM. Resistance to systemic therapies in clear cell renal cell carcinoma: mechanisms and management strategies. Mol Cancer Ther 2018;17:1355–64.
4. Jonasch E, Walker CL, Rathmell WK. Clear cell renal cell carcinoma ontogeny and mechanisms of lethality. Nat Rev Nephrol 2021;17:245–61.
5. Cancer Genome Atlas Research N. Comprehensive molecular characterization of clear cell renal cell carcinoma. Nature 2013;499:43–9.
6. Linehan WM, Ricketts CJ. The cancer genome atlas of renal cell carcinoma: findings and clinical implications. Nat Rev Urol 2019;16:539–52.
7. Gerlinger M, Horswell S, Larkin J, Rowan AJ, Salm MP, Varela I, et al. Genomic architecture and evolution of clear cell renal cell carcinomas defined by multiregion sequencing. Nat Genet 2014;46:225–33.
8. Kaelin WG Jr. The VHL tumor suppressor gene: insights into oxygen sensing and cancer. Trans Am Clin Climatol Assoc 2017;128:298–307.
9. de Vivar Chevez AR, Finke J, Bukowski R. The role of inflammation in kidney cancer. Adv Exp Med Biol 2014;816:197–234.
10. Diaz-Montero CM, Rini BI, Finke JH. The immunology of renal cell carcinoma. Nat Rev Nephrol 2020;16:721–35.
11. Tan W, Hildebrandt MA, Pu X, Huang M, Lin J, Matin SF, et al. Role of inflammatory related gene expression in clear cell renal cell carcinoma development and clinical outcomes. J Urol 2011;186:2071–7.
12. Greten FR, Grivennikov SI. Inflammation and cancer: triggers, mechanisms, and consequences. Immunity 2019;51:27–41.
13. Kuo CY, Lin CH, Hsu T. VHL inactivation in precancerous kidney cells induces an inflammatory response via ER stress-activated IRE1alpha signaling. Cancer Res 2017;77:3406–16.
14. Qian BZ, Pollard JW. Macrophage diversity enhances tumor progression and metastasis. Cell 2010;141:39–51.
15. Mantovani A, Marchesi F, Malesci A, Laghi L, Allavena P. Tumour-associated macrophages as treatment targets in oncology. Nat Rev Clin Oncol 2017;14:399–416.
16. Pathria P, Louis TL, Varner JA. Targeting tumor-associated macrophages in cancer. Trends Immunol 2019;40:310–27.
17. Orecchioni M, Ghosheh Y, Pramod AB, Ley K. Macrophage polarization: different gene signatures in M1(LPS+) vs. classically and M2(LPS-) vs. alternatively activated macrophages. Front Immunol 2019;10:1084.
18. Yang M, McKay D, Pollard JW, Lewis CE. Diverse functions of macrophages in different tumor microenvironments. Cancer Res 2018;78:5492–503.
19. Ruffell B, Affara NI, Coussens LM. Differential macrophage programming in the tumor microenvironment. Trends Immunol 2012;33:119–26.
20. Pritchett TL, Bader HL, Henderson J, Hsu T. Conditional inactivation of the mouse von Hippel–Lindau tumor suppressor gene results in wide-spread hyperplastic, inflammatory and fibrotic lesions in the kidney. Oncogene 2015;34:2631–9.
21. Nguyen-Tran HH, Nguyen TN, Chen CY, Hsu T. Endothelial reprogramming stimulated by oncostatin m promotes inflammation and tumorigenesis in VHL-deficient kidney tissue. Cancer Res 2021;81:5060–73.
22. Chevrier S, Levine JH, Zanotelli VRT, Silina K, Schulz D, Bacac M, et al. An immune atlas of clear cell renal cell carcinoma. Cell 2017;169:736–49.
23. Vuong L, Kotecha RR, Voss MH, Hakimi AA. Tumor microenvironment dynamics in clear-cell renal cell carcinoma. Cancer Discov 2019;9:1349–57.
24. Hsouna A, Nallamothu G, Kose N, Guinea M, Dammai V, Hsu T. Drosophila von Hippel-Lindau tumor suppressor gene function in epithelial tubule morphogenesis. Mol Cell Biol 2010;30:3779–94.
25. Cho H, Seo Y, Loke KM, Kim SW, Oh SM, Kim JH, et al. Cancer-stimulated CAFs enhance monocyte differentiation and protumoral TAM activation via IL6 and GM-CSF secretion. Clin Cancer Res 2018;24:5407–21.
26. Yu J, Carroll TJ, McMahon AP. Sonic hedgehog regulates proliferation and differentiation of mesenchymal cells in the mouse metanephric kidney. Development 2002;129:5301–12.
27. Gu YF, Cohn S, Christie A, McKenzie T, Wolff N, Do QN, et al. Modeling renal cell carcinoma in mice: Bap1 and Pbrm1 inactivation drive tumor grade. Cancer Discov 2017;7:900–17.
28. Harlander S, Schonenberger D, Toussaint NC, Prummer M, Catalano A, Brandt L, et al. Combined mutation in Vhl, Trp53 and Rb1 causes clear cell renal cell carcinoma in mice. Nat Med 2017;23:869–77.
29. Feng X, Zhang L, Tu W, Cang S. Frequency, incidence and survival outcomes of clear cell renal cell carcinoma in the United States from 1973 to 2014: A SEER-based analysis. Medicine (Baltimore) 2019;98:e16684.
30. Shen H, Liu J, Chen S, Ma X, Ying Y, Li J, et al. Prognostic value of tumor-associated macrophages in clear cell renal cell carcinoma: a systematic review and meta-analysis. Front Oncol 2021;11:657318.
31. Zimmerman KA, Bentley MR, Lever JM, Li Z, Crossman DK, Song CJ, et al. Single-cell RNA sequencing identifies candidate renal resident macrophage gene expression signatures across species. J Am Soc Nephrol 2019;30:767–81.
32. Beyer M, Mallmann MR, Xue J, Staratschek-Jox A, Vorholt D, Krebs W, et al. High-resolution transcriptome of human macrophages. PLoS One 2012;7:e45466.
33. Martinez FO, Gordon S, Locati M, Mantovani A. Transcriptional profiling of the human monocyte-to-macrophage differentiation and polarization: new molecules and patterns of gene expression. J Immunol 2006;177:7303–11.
34. Sawant KV, Poluri KM, Dutta AK, Sepuru KM, Troshkina A, Garofalo RP, et al. Chemokine CXCL1 mediated neutrophil recruitment: role of glycosaminoglycan interactions. Sci Rep 2016;6:33123.
35. Jones SA, Jenkins BJ. Recent insights into targeting the IL-6 cytokine family in inflammatory diseases and cancer. Nat Rev Immunol 2018;18:773–89.
36. Mandriota SJ, Turner KJ, Davies DR, Murray PG, Morgan NV, Sowter HM, et al. HIF activation identifies early lesions in VHL kidneys: evidence for site-specific tumor suppressor function in the nephron. Cancer Cell 2002;1:459–68.
37. Fitzgerald JP, Nayak B, Shanmugasundaram K, Friedrichs W, Sudarshan S, Eid AA, et al. Nox4 mediates renal cell carcinoma cell invasion through hypoxia-induced interleukin 6- and 8-production. PLoS One 2012;7:e30712.
38. Onnis B, Rapisarda A, Melillo G. Development of HIF-1 inhibitors for cancer therapy. J Cell Mol Med 2009;13:2780–6.
39. Lee FD. The role of interleukin-6 in development. Dev Biol 1992;151:331–8.

40. Withy RM, Rafield LF, Beck AK, Hoppe H, Williams N, McPherson JM. Growth factors produced by human embryonic kidney cells that influence megakaryopoiesis include erythropoietin, interleukin 6, and transforming growth factor-beta. J Cell Physiol 1992;153:362–72.
41. Choy EH, De Benedetti F, Takeuchi T, Hashizume M, John MR, Kishimoto T. Translating IL-6 biology into effective treatments. Nat Rev Rheumatol 2020;16:335–45.
42. Johnson DE, O'Keefe RA, Grandis JR. Targeting the IL-6/JAK/STAT3 signalling axis in cancer. Nat Rev Clin Oncol 2018;15:234–48.
43. Dongre A, Weinberg RA. New insights into the mechanisms of epithelial-mesenchymal transition and implications for cancer. Nat Rev Mol Cell Biol 2019;20:69–84.
44. Bonde AK, Tischler V, Kumar S, Soltermann A, Schwendener RA. Intratumoral macrophages contribute to epithelial-mesenchymal transition in solid tumors. BMC Cancer 2012;12:35.
45. Su S, Liu Q, Chen J, Chen J, Chen F, He C, et al. A positive feedback loop between mesenchymal-like cancer cells and macrophages is essential to breast cancer metastasis. Cancer Cell 2014;25:605–20.
46. Suarez-Carmona M, Lesage J, Cataldo D, Gilles C. EMT and inflammation: inseparable actors of cancer progression. Mol Oncol 2017;11:805–23.
47. Taniguchi S, Elhance A, Van Duzer A, Kumar S, Leitenberger JJ, Oshimori N. Tumor-initiating cells establish an IL-33-TGF-beta niche signaling loop to promote cancer progression. Science 2020;369:eaay1813.
48. Massague J. TGFbeta in Cancer. Cell 2008;134:215–30.
49. Hunter CA, Jones SA. IL-6 as a keystone cytokine in health and disease. Nat Immunol 2015;16:448–57.
50. Kovaleva OV, Samoilova DV, Shitova MS, Gratchev A. Tumor associated macrophages in kidney cancer. Anal Cell Pathol (Amst) 2016;2016:9307549.
51. Xu L, Zhu Y, Chen L, An H, Zhang W, Wang G, et al. Prognostic value of diametrically polarized tumor-associated macrophages in renal cell carcinoma. Ann Surg Oncol 2014;21:3142–50.
52. Alberti L, Thomachot MC, Bachelot T, Menetrier-Caux C, Puisieux I, Blay JY. IL-6 as an intracrine growth factor for renal carcinoma cell lines. Int J Cancer 2004;111:653–61.
53. Horiguchi A, Oya M, Shimada T, Uchida A, Marumo K, Murai M. Activation of signal transducer and activator of transcription 3 in renal cell carcinoma: a study of incidence and its association with pathological features and clinical outcome. J Urol 2002;168:762–5.